Unterschrift des Betreuers

TECHNISCHE UNIVERSITÄT WIEN
Vienna University of Technology

DIPLOMARBEIT

Influence of testing frequency on the fatigue properties of polycrystalline copper

Ausgeführt am
Institut für Festkörperphysik
der Technischen Universität Wien

unter Anleitung von
Ao.Univ.Prof.i.R. Dipl.-Ing. Dr.techn. Elmar TSCHEGG

in Zusammenarbeit mit dem
Institut für Physik und Materialwissenschaft
der Universität für Bodenkultur

durch
Andrea PERLEGA
Matrikelnummer: 0349024

May 2015

Unterschrift

Abstract

The influence of cycling frequency on the fatigue properties of polycrystalline copper in the very high cycle regime is investigated. Tests were performed with servohydraulic testing equipment at 20 Hz and using ultrasonic testing equipment operating at approximately 20 kHz. SN-tests and plastic strain amplitude measurements were performed. A significant difference in the results is found. Other influences than testing frequency are discussed and the results are compared with results from literature.

Zusammenfassung

Der Einfluss der Testfrequenz auf das Ermüdungsverhalten von polykristallinem Kupfer wird untersucht. Tests wurden bei 20 Hz mit einer servohydraulischen Prüfmaschine und bei 20 kHz mittels einer Ultraschall-Ermüdungs-Anlage durchgeführt. Neben der Messung von Wöhlerkurven wurde auch die plastische Dehnungsamplitude gemessen. Ein signifikanter Unterschied in den Ergebnissen der Tests konnte festgestellt werden. Über den Einfluss der Testfrequenz hinaus werden auch andere mögliche Einflüsse diskutiert und ein Vergleich mit Ergebnissen aus der Literatur durchgeführt.

Danksagung

Für die Unterstützung und die Betreuung dieser Diplomarbeit möchte ich Frau Prof. Dr. Stefanie Stanzl-Tschegg herzlich danken. Sie hat mir die Freiheit gegeben mich in die Themen meines Interesses zu vertiefen und mich in vielerlei Hinsicht gefördert. Unter anderem dadurch, dass sie mir die Chance gegeben hat an mehreren facheinschlägigen Konferenzen und Tagungen teilzunehmen. Die Inputs die ich in diesem Rahmen erhalten habe, haben maßgeblich zu dieser Arbeit beigetragen. Nicht zuletzt hat mir Prof. Dr. Stefanie Stanzl-Tschegg durch die Anstellung in ihrer Arbeitsgruppe auch in finanzieller Hinsicht die Möglichkeit geboten mein Studium abzuschließen. Ohne ihre Unterstützung wäre diese Arbeit nicht zustande gekommen.

Herrn Prof. Dr. Elmar Tschegg danke ich für die Betreuung und für sein Bemühen, dass diese Arbeit zustande kam.

Den MitarbeiterInnen des Instituts für Physik und Materialwissenschaft der Universität für Bodenkultur möchte ich für ihre Unterstützung und ihren Rat danken. Bei Fragen konnte ich mich immer an sie wenden und bekam die Hilfe und Unterstützung, die ich brauchte.

Danken möchte ich auch meinen Freundinnen dafür, dass sie immer an mich geglaubt haben und mich das auch wissen lassen haben. Dafür, dass sie mich ermutigt haben weiter zu machen.

Contents

Chapter 1

Fatigue

A material can fail below its ultimate tensile strength and even below its yield strength. Two different mechanisms (namely fatigue and creep) can lead to such failure. Fatigue describes failure below the material's strength due to repeated loading [1], whereas creep is failure due to a static load below the material's strength [2]. Fatigue is described usually in terms of applied load versus number of cycles until failure, whilst creep is described by the time a static load is applied until failure. In engineering practice, this is taken into account by adding safety factors to the calculations.

Fatigue has been investigated since the nineteenth century. The Industrial Revolution led to a rapid development of technology and increased demands on components. First reports about fatigue test results and fatigue failure were already published in the first half of the nineteenth century. Fatigue failure in railway axles was a common problem leading to many fatal accidents. These failures gave a first rise to the scientific investigation of fatigue. Most commonly known is the work of August Wöhler in the second half of the nineteenth century. After World War II a number of aircraft crashes resulting from fatigue failure raised further interest in fatigue. Since then, fatigue is a field constantly investigated. More detailed information on the history of fatigue give [3, 4].

Within fatigue it is often distinguished between several regimes. These are namely low cycle fatigue (LCF), high cycle fatigue (HCF), very high cycle fatigue (VHCF) and sometimes even ultra-high cycle fatigue (UHCF). They are discriminated by number of cycles to failure but there is no sharp criterion to distinguish these regimes. The LCF regime is characterized by macroplasticity occurring in every cycle. It is usually limited to some 10^4 or 10^5 cycles. The HCF regime is more related to elastic behaviour on an macroscopic scale [5]. As failure is also found for number of cycles greater than $5 \cdot 10^7$ or 10^8 in many materials, the term VHCF has been established for this regime. In the UHCF regime the number of cycles to failure can reach 10^{10} cycles or even more. The

plastic strain amplitudes are very low (10^{-7} or even less). Such small plastic strains only cause failure if they are repeatedly applied and damage can accumulate [6].

1.1 Elastic and Plastic Deformation

Considering a perfect crystal, elastic deformation can be defined as the as the sum of the elastic deformation of all unit-cells. Without an external stress atoms are in their equilibrium position (in the crystal potential). If a (small) force is applied, atoms deviate from their equilibrium positions. If the force is removed, the atoms take their initial equilibrium positions. The elastic deformation is therefore reversible.

When a solid is deformed elastically, its crystal lattice (namely the lattice spacing) is changed. But when the applied stress is removed, the lattice spacing takes its initial value again. The initial lattice cannot be distinguished from the lattice after removing the applied stress. On a macroscopic level the strain ε is proportional to the applied stress σ with Young's modulus E as a proportionality factor. Hooke's law

$$\sigma = E \cdot \varepsilon \tag{1.1}$$

describes the behaviour.

The crystal potential is built by many potential wells which are possible (equilibrium) positions for the atoms. If the force is high enough, the atoms can move to another potential well. If the force is removed, the atoms will not be in their initial equilibrium position but in a different potential well. The deformation is still present if the force is removed.

The macroscopic observation of stresses and strains is in good agreement with this model. But if elasticity and plasticity are observed at a smaller scale the linear elastic regime is only an approximation. Already for small stresses nonlinear elastic behaviour and plastic deformation (strain localization by movement of dislocations) occurs. Nonlinear elasticity is not limited to high strains only [1]. Plastic deformation occurs also at stress levels lower than the macroscopic flow stress [7].

The strain resulting from an applied stress can be written as the sum of elastic and plastic strain.

$$\varepsilon = \varepsilon_{el} + \varepsilon_{pl} \tag{1.2}$$

If a load is applied, the strain measured will not show a perfectly linear behaviour in relation to the applied stress. If the applied load is reversed and applied again, stress

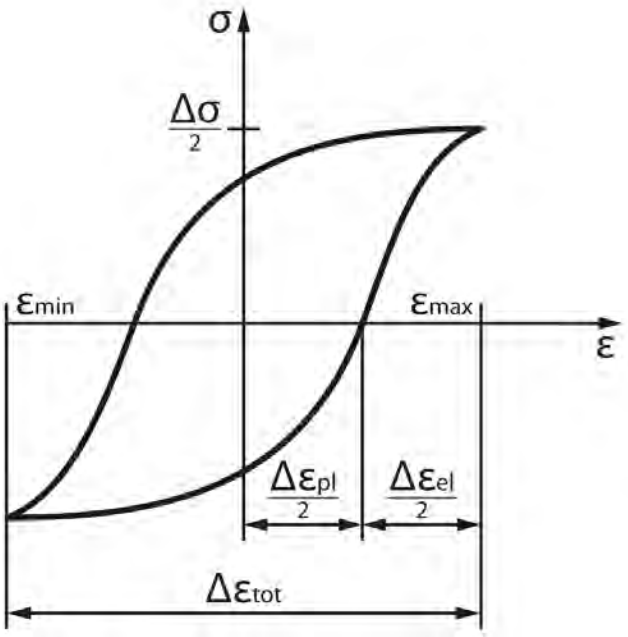

FIGURE 1.1: Hystersis loop according to [4].

and strain will form a hysteresis loop. Figure 1.1 shows such an idealized hysteresis loop. The hysteresis loop's slope is defined by the Young's modulus E. Its width is related to the plastic strain ε_{pl}. The hysteresis loop's shape is depending on the material, the test setup (e.g. test control, testing frequency) and an eventual prestraining history [1].

A perfect solid would be a single crystal of infinite size with no crystal defects. A real solid however has several crystal defects, starting with the interfaces between the solid and its surrounding and several other defects are also always present. These are namely:

Point defects: Including vacancies and self-interstitials, substitutional and interstitial foreign atoms.

Linear defects: Including edge dislocations and screw dislocation as well as mixed forms, which are most often found.

Interfacial defects: Including external surfaces, grain boundaries, phase boundaries and twin boundaries.

Concerning fatigue, dislocations are of great importance. They can move within the crystal lattice. Dislocations prefer certain crystallographic planes and directions for their motion. These are named slip planes and slip directions and they constitute a slip system. The atomic lattice is distorted around the dislocations leading to lattice strains. These strain fields interact with each other. In the case of two opposite strain fields this interaction leads to dislocation annihilation [8].

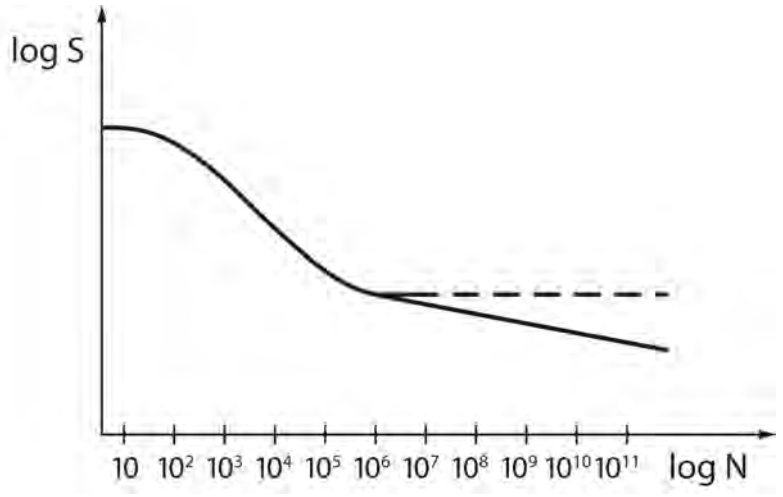

FIGURE 1.2: Illustration of an idealized SN-Curve according to [4].

1.2 SN-Curve

In engineering practice the SN-diagram is the most used tool to estimate fatigue failure [1]. The stress amplitude (S or $\Delta\sigma/2$) is therefore plotted double logarithmically over the number of cycles to failure (N or N_f). Specimens that did not show failure within a specified limit of number of cycles are called run-outs.

The Basquin relation

$$S^k \cdot N = constant \tag{1.3}$$

describes the relation between stress amplitude and number of cycles to failure mathematically. $1/k$ describes the slope for the linear part of an SN-diagram [5].

Figure 1.2 shows an idealized SN-curve. For some materials a fatigue limit at a certain number of cycles is expected. Others do not exhibit a fatigue limit even at very high numbers of cycles. Mild steels and other strain-ageing materials are examples for materials exhibiting a fatigue limit. The SN-curve shows a plateau represented in Figure 1.2 by a dashed line. Stress amplitudes smaller than the fatigue limit are supposed to lead to infinite life. Many high strength steels, aluminium alloys and other materials (including copper [9]) do not exhibit such a plateau. If the stress amplitude is decreased the number of cycles to failure increases but failure still occurs. This behaviour is represented by a solid line in Figure 1.2. An endurance limit has to be defined for a given number of cycles for these materials [10]. It has to be noted that the fatigue limit cannot be safely extrapolated from measurements performed at lower number of cycles [11].

1.3 Coffin-Manson-Diagram

Fatigue tests have been performed in the past in various ways of test control. Results of tests conducted in stress control are usually plotted in an SN-diagram. Results of tests performed with plastic strain amplitude as controlling parameter are usually plotted in a Coffin-Manson diagram, where the plastic strain amplitude $\Delta\varepsilon_{pl}/2$ is double logarithmically plotted over the number of cylces to failure N_f. Coffin and Manson proposed that the fatigue life is characterized by the plastic strain amplitude [10]. The Coffin-Manson relationship

$$\frac{\Delta\varepsilon_{pl}}{2} = \varepsilon'_f \cdot (2N_f)^c \tag{1.4}$$

describes the relation between plastic strain amplitude $\Delta\varepsilon_{pl}/2$ and reversals to failure $2N_\mathrm{f}$ mathematically. ε'_f is here the fatigue ductility coefficient and c the fatigue ductility exponent.

To be able to compare different test results, a transformation of the obtained data is necessary. To transform results from stress controlled tests, the plastic strain amplitude at saturation at the individual stress levels is used. The question of the legitimacy of such a transformation has already been posed e.g. by Lukáš et al. [12] in the 1970ies. They came to the conclusion that such a transformation would work perfect for a material that does neither exhibit cyclic hardening nor softening. For materials exhibiting a short and limited range of cyclic hardening or softening in their fatigue life (e.g. copper), the transformation works still good. Only for materials with a very pronounced or long lasting cyclic hardening or softening period the transformation is not permissible. Investigating the applicability of such a transformation in the HCF regime, they found that for $N_\mathrm{f} < 10^7$ cycles the Coffin-Manson relationship is valid. Mughrabi [13] assumes that the Coffin-Manson relationship is also valid in the UHCF regime.

1.4 Persistent Slip Bands

If a polycrystalline solid is subjected to cyclic loading, cyclic slip occurs. The applied load induces a cyclic shear stress in every grain. The magnitude of the shear stress is depending on the grain's size, shape and crystallographic orientation (namely the orientation of possible slip planes with respect to the loading axis) as well as the material's elastic anisotropy.

At the free surface fewer constraints on slip are present than inside the solid where a grain is completely surrounded by neighbouring grains. Therefore, slip will occur preferably in surface grains as slip can occur there at lower stress levels than in internal grains. If

slip occurs, a slip step is generated. The newly formed surface is (immediately) covered by an oxide layer. Also strain hardening occurs. Due to strain hardening, a larger shear stress is present in the reversed cycle. Also reversed slip will not act in the exact same slip plane as the oxide layer hinders the reversed movement. A parallel slip plane will be activated. Rerunning the loading and unloading cycle this process is repeated forming a slip band [5]. It is noted that although one (primary) slip system is dominant, slip may occur on several slip systems at low amplitudes [14].

Thompson et al. [15] tested commercially pure copper at a testing frequency of 1000 Hz. Interrupting the fatigue process and electro-polishing the specimens, they found that some of the slip bands that had formed were reappearing. These were named persistent slip bands (PSBs) and cracks eventually initiated at some of these PSBs.

The dislocation structure within a PSB is significantly different from the matrix. A PSB has a lamellar structure, which can cover in the case of single crystals its entire cross section. Dislocation walls divide the PSB lamella into channels. This structure is often described as a ladder-like structure. Plastic deformation mainly caused by glide of screw dislocations is localized in these channels [10].

PSBs are closely linked to fatigue failure of pure metals. The shear displacement along a slip band results in a surface roughening. The generated intrusions act as stress concentrators promoting additional slip and crack nucleation [10]. For commercially pure copper with a grain size of 25 µm tested in plastic strain control the lowest plastic strain amplitude where PSBs were found was $5{\cdot}10^{-5}$ (corresponding to a stress amplitude of 56 MPa) [16]. As cracks mainly initiate at PSBs in the VHCF regime, this finding was related to the presence of a fatigue limit below which no failure will occur. Laird [17] reports tests on copper single crystals showing that below a certain strain amplitude PSBs were absent. Therefore, he suggests the existence of a fatigue limit. Lukáš and Kunz [6] also supposed extrapolating HCF data that in the UHCF regime there would be no PSBs in the UHCF regime, although they expected a failure mechanism related to cyclic slip irreversibility.

More recent investigations [18–22] using ultrasonic fatigue testing equipment operating in total strain control showed that fatigue damage appears also below this (so named) "conventional" PSB threshold. At a nominal stress amplitude of 34 MPa (corresponding to a plastic strain amplitude of $2.9 \cdot 10^{-6}$) one single slip band is reported within $1.3 \cdot 10^{10}$ cycles. PSB formation is therefore not only depending on the applied load but also on the loading history, namely the number of cycles already endured. If the load is lower, higher numbers of cycles are needed to create a PSB. These PSBs generated at very low amplitudes did not lead to failure, namely no failure occurred for nominal

stress amplitudes of 92.2 MPa (corresponding to a plastic strain amplitude of $1.85 \cdot 10^{-5}$) or smaller.

1.5 Cracks

Cracks play a major role in the fatigue process. The fatigue life can be divided into two periods. A crack initiation period and a crack growth period which is followed by failure [5]. The mechanism of crack initiation are therefore of great interest. Cracks can nucleate at grain boundaries or twin boundaries, inclusions, microstructural or compositional inhomogeneities or microscopic or macroscopic stress concentrators [10]. In the following findings on fatigue cracks in copper are summarized:

Figueroa and Laird [23] found that cracks do not preferably nucleate at PSBs but at grain boundaries intersecting with a PSB. They performed tests at a plastic strain amplitude of 10^{-3} and 10^{-4} and studied the evolution of the surface topology (including slip band evolution and crack nucleation) and dislocation structures. The plastic strain amplitude of the current tests lies clearly lower (for the ultrasonic fatigue tests it was in the range of $5 \cdot 10^{-6}$ to $1.5 \cdot 10^{-5}$, for the 20 Hz tsts it was in the range of $4 \cdot 10^{-5}$ to $2 \cdot 10^{-4}$, for details see Chapter 3.3).

Stanzl-Tschegg et al. [19, 20, 22] reported a similar behaviour for tests conducted at 20 kHz. They found cracks at grain boundaries originating from the intersection of a primary slip band with the grain boundary as well as small stage I cracks originating from deep intrusions at the interface between PSB and matrix. Also Phung et al. [24] and Awatani et al. [9] reported cracks nucleating at the intersection of PSBs with grain boundaries.

1.6 Copper

Copper is a face-centred cubic (fcc) metal and is available in high purity. It exhibits wavy slip and has twelve slip systems. The main slip plane is $\{1\,1\,1\}$ and the slip direction is $\langle 1\,\bar{1}\,0 \rangle$.

Numerous papers exist that investigate the fatigue behaviour of copper. It is not possible to give a complete overview within this thesis. Therefore, only a brief overview on the investigations performed on copper relevant for this thesis will be given in the following:

Since the second half of the twentieth century the investigation of copper's fatigue properties is an important part of fundamental fatigue research. The influence of testing itself

(mainly loading procedure and test control) was investigated [e.g. 25, 26]. First investigations where performed on copper single crystals orientated for single slip [e.g. 27, 28]. These investigations focused on the evolution and development of PSBs and their role in the fatigue process. The dislocation structure of the PSBs was investigated using transmission electron microscopy (TEM) [e.g. 28–31]. Subsequently also polycrystals were investigated. It was widely discussed how the findings for single crystals can be applied to polycrystals [e.g. 16].

Awatani et al. [9] performed first investigations using ultrasonic fatigue testing technique already in the 1970ies showing that copper has no fatigue limit. Stanzl-Tschegg et al. [19, 20] investigated the slip band evolution in the VHCF regime. Lukáš et al. [32] performed investigations on ultra-fine grained copper in the VHCF regime.

1.7 Cyclic Hardening and Cyclic Softening

Generally the materials behaviour under cyclic load is determined by its mechanical history [1]. Depending on the test control, cyclic hardening and softening are defined as follows: In stress control the strain is decreasing when cyclic hardening occurs. It is increasing for cyclic softening. In strain control the stress is increasing when cyclic hardening occurs whereas it is decreasing when cyclic softening occurs [10].

If an annealed specimen is tested in stress control, often a typical behaviour can be observed: After initial hardening, the plastic strain amplitude is constant over a wide range of cycles. This range often takes most of the specimen's lifetime. It is named saturation behaviour. A prestrained material on the other hand often behaves differently. An initial softening is followed by saturation. Neither can be safely predicted whether cyclic hardening or softening will occur nor its extent as the microstructural processes determining the behaviour are highly complex [1].

1.8 Frequency Effects

When testing at low amplitudes where high numbers of cycles are achieved, it is more convenient to test at high testing frequencies. Using ultrasonic fatigue testing equipment, the testing frequency (here approx. 19 kHz) is about thousand to tenthousand times higher than conventional testing frequencies of servohydraulic testing systems.

The open question in the sense of comparability with conventional testing frequencies is, whether this change to higher testing frequency is permissible or not. If in-service

frequencies are similar to the testing frequency used, a possible frequency influence does not need to be considered. But if test results should be comparable to results obtained at other testing frequencies or if in-service frequencies differ significantly, the question if a frequency effect is acting on the results obtained has to be posed.

It is mentioned by Stanzl-Tschegg that no frequency influence on the fatigue results is expected for most technical alloys if the testing conditions are comparable [11]. For materials with high ductility and strain-rate sensitivity, a frequency effect may be expected nevertheless. Investigating the influence of loading frequency using body-centred cubic (bcc) and hexagonal close-packed (hcp) metals, Papakyriacou et al. [33] found a real frequency effect for Tantalum.

Although copper as an fcc metal is normally viewed as frequency insensitive, some investigations on a possible frequency effect have been performed. Most of them were performed at conventional testing frequencies fairly below 100 Hz.

Yan et al. [31] found investigating copper single crystals that after an initial ramp loading procedure the plastic strain amplitude increased strongly if the testing frequency was reduced (from 34 to 2 Hz). A reduction of frequency of one order of magnitude had a marked effect on the nucleation behaviour of PSBs. PSBs nucleated more easily for lower testing frequencies.

Mayer and Laird [34] investigated the influence of testing frequency (in the range of 0.5 to 8 Hz) on both saturation behavior and cyclic plasticity following saturation. They conducted stress controlled tests in ramp loading and found an influence of cyclic frequency on the saturation behavior. For stress amplitudes higher than 90 MPa a higher plastic strain amplitude is achieved if tested at 0.5 Hz compared to 2 or 8 Hz. A pronounced influence of testing frequency on the strain localization was found. It started earlier and was more pronounced for lower frequencies. Also a higher density of slip markings was found if tests were performed at lower frequencies.

Awatani et al. [9] investigated whether or not a fatigue limit could be found in fcc materials using copper as testing material and ultrasonic fatigue testing equipment operating at 17.7 kHz. They pose the question whether the fatigue mechanism is changed by the testing frequency. Different from iron and brass, no differences could be found in annealed copper as slip bands also grew during the test. PSBs were formed and the dislocation structure was similar to that obtained in tests at conventional testing frequencies. Therefore, they assumed that the fatigue mechanisms are the same at ultrasonic frequencies and at lower frequencies.

Performing SN-tests at ultrasonic frequencies, Stanzl-Tschegg and Schönbauer [19] found a fatigue limit for 10^{10} cycles at 92.2 MPa, which is significantly higher than the fatigue

limits at conventional testing frequencies reported in literature. Measuring plastic strain amplitudes at 20 Hz and 19 kHz, they found that the plastic strain amplitudes were essentially lower for ultrasonic frequencies [18].

Investigating the different forms of fatigue damage occurring in the UHCF regime, Weidner et al. [21] pose the question of a frequency dependence of the PSB threshold amplitudes. The PSB formation threshold for conventional testing frequencies is significantly lower than that reported for ultrasonic frequencies [18–20]. A frequency effect related to the higher strain rate at ultrasonic frequencies is therefore suggested by Weidner et al. [21]: The formation of PSBs is linked to the destabilization and breakdown of the initial dipolar vein dislocation structure leading to the known ladder-like structure of PSBs. This destabilization starts as a local destabilization, which spreads if the time before the next destabilizing event is short enough that "healing" is prohibited. If the testing frequency is increased, this time is reduced and the spreading of local instabilities becomes more likely.

Marti et al. [35] investigated the frequency effect in the very high cycle regime for polycrystalline copper[1]. SN-tests at conventional frequencies are compared to Phung et al.'s test results [24] at ultrasonic frequencies. Tests were carried out with Oxygen-Free High-Conductivity (OFHC) copper (purity of 99.99 %) with a grain size of 30 µm, but no information on test control or loading procedure (e.g. ramp loading) is available. The test results for conventional testing frequencies (namely 10, 20 and 100 Hz) are summarized in one SN-diagram. A clear difference in the results is visible. For a given stress amplitude, the fatigue life is higher if tested with 20 kHz. Furthermore, the evolution of slip markings was studied interrupting the fatigue test and investigating the specimen surface. It was found that the amount of slip markings for a given stress amplitude is higher when tested at 100 Hz then if tested at 20 kHz.

Mason and Wood [36] investigated the differences in how slip spreads and how fatigue cracks propagate for conventional testing frequencies of about 28 Hz and ultrasonic testing frequencies of 17 kHz. They found that testing at room temperature at low strain amplitudes (as small as 10^{-4}) using ultrasonic fatigue testing equipment isolated single slip bands appeared which turned into micro-cracks during testing whereas slip bands covered the whole grain if tested at conventional frequencies.

[1] The results were presented at the International Conference on Very High Cycle Fatigue in Chengdu (China) in October 2014. Their work was performed at the same time the tests for this master's thesis were done.

1.9 Scatter

Fatigue always shows scatter although some sources of scatter are minimized in laboratory tests (e.g. by using material from one batch, applying the same specimen shape, identical specimen preparation, similar surface quality). In general scatter is smaller at high stress amplitudes and becomes larger at low stress amplitudes [5].

It is necessary to test a sufficient number of specimens to get information on the statistical variation. If the number of tested specimens is too small, still an average curve can be drawn which corresponds to a 50 % probability of failure.

In the following the procedure of calculating the SN-curves for fracture probabilities of 10, 50 and 90 % are described:

To calculate the 50 % fracture probability, the Basquin equation (see Chapter 1.2) is calculated by fitting the data of all stress levels which showed failure exclusively. Stress levels including run-out specimens cannot be used for the calculation. A power law distribution in the form of

$$N = a \cdot x^b = a \cdot x^{-\frac{1}{k}} \tag{1.5}$$

is used to fit the data and receive k.

All results are shifted to one stress level S_1 using the Basquin equation and a log-normal probability plot is drawn from these results. The number of cycles to failure corresponding to the 10, 50 and 90 % fracture probability ($N(10)$, $N(50)$ and $N(90)$) can be read from this plot. Using these, the constants for the equations of the SN-curves of 10, 50 and 90 % fracture probability are obtained:

$$\frac{\Delta\sigma}{2} \cdot N^k = C(10) = S_1 \cdot N(10)^k \tag{1.6}$$

$$\frac{\Delta\sigma}{2} \cdot N^k = C(50) = S_1 \cdot N(50)^k \tag{1.7}$$

$$\frac{\Delta\sigma}{2} \cdot N^k = C(90) = S_1 \cdot N(90)^k \tag{1.8}$$

Chapter 2

Material and Test Setup

2.1 Material

The material tested is commercially pure Electrolytic-Tough-Pitch Copper (Cu-ETP) with an ultimate tensile strength of 271 MPa and a yield strength of 203 MPa (condition at delivery). It was received in rods with a diameter of 15 mm and a length of 2 m. The purity of the material was 99.99 % (see Appendix A). In general a purity of 99.95 % is demanded for Cu-ETP. It is produced by electrolytic refining and contains oxygen (in contrast to several types of oxygen free copper).

To ensure comparability, all specimens for the present tests were produced from material of one batch. Specimens were ground, electropolished and heat treated (details can be found in Chapter 2.3.1 and 2.3.2). To ensure comparability with former tests [18–22, 37, 38] the same material was used but the batch differed. The heat treatment was chosen such that the grain size was of the same order. The Young's modulus was determined after heat treatment dynamically at ultrasonic frequency. For all subsequent calculations E =127.7 GPa was used.

Using images of specimens tested by Eichinger [37] and Schönbauer [38], the former tests' grain size determined (using the average grain intersect method DIN 2624) is 36 µm. The mean grain size of the present tests' specimens was 39 µm. Figure 2.1 shows the microstructure obtained. The grain size was measured using the average grain intersect method specified in DIN 2624 (details are listed in Appendix B).

Tests were performed using annealed specimens. Additionally four tests at 20 Hz were performed using prestrained specimens. These specimens have been accidently slightly bent and were straightened before testing. These tests were only performed to get a

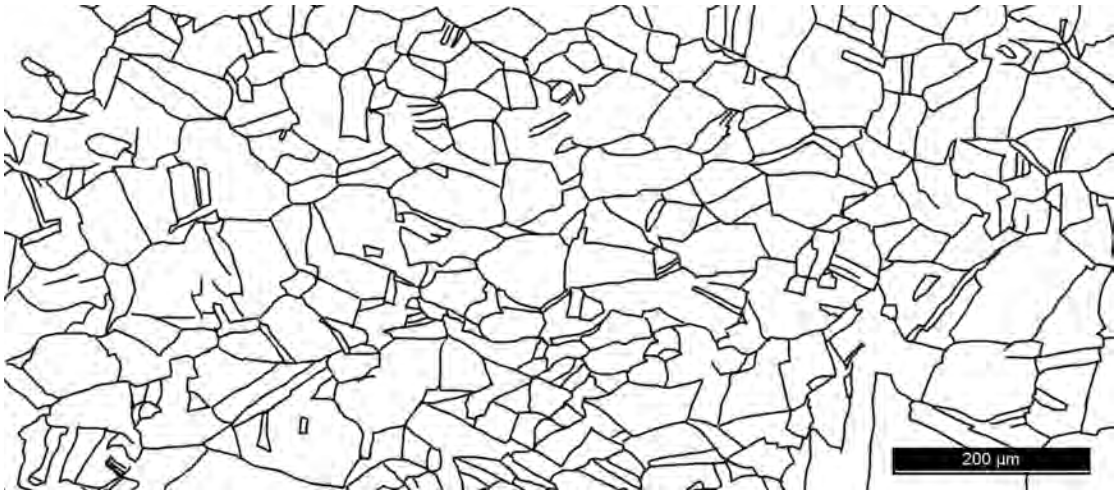

FIGURE 2.1: Microstructure.

deeper insight on effects on the test results (details are described in Chapter 4.2). They are not considered as valid tests.

2.2 Specimen Shape

Different specimen shapes were used to carry out different types of tests.

For the fatigue tests at 20 Hz, an hourglass shaped specimen with a diameter of 3 mm in the centre of the specimen was used. The specimen shape is given in Figure 2.2. For the fatigue tests at approximately 19 kHz, also an hourglass shaped specimen of the same general shape was used, but the specimen length was chosen such that the specimen vibrated in resonance at a frequency of approximately 19 kHz. The specimen shape is given in Figure 2.3.

For the thermoelectric measurements of the plastic strain amplitude at ultrasonic frequency, a specimen as specified in Figure 2.4 was used. The hourglass shaped specimen is not suitable for this measurement as the heat generated due to plastic deformation is transported to the specimen ends rapidly. Therefore, the temperature change cannot be measured with sufficient accuracy. The plastic strain amplitude is underestimated if hourglass shaped specimens are used for this measurement. The specimen shape was chosen according to the specimen shape described in [38] and [19]. As the material was available in rods with a diameter of 15 mm it was not necessary to solder the specimen into a mounting socket to enable mounting into the fatigue testing setup. It was possible to machine horn shaped specimens.

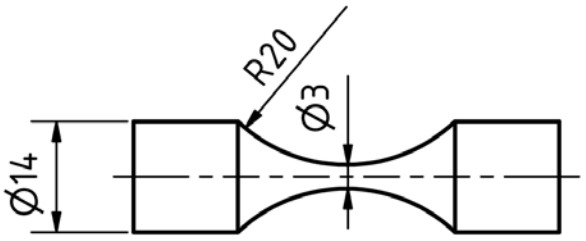

FIGURE 2.2: Specimen Shape for 20 Hz tests.

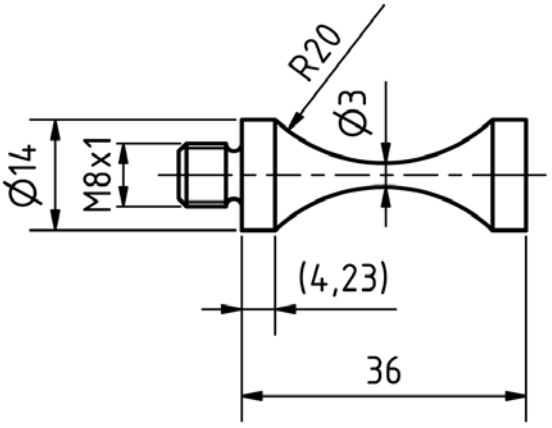

FIGURE 2.3: Specimen Shape for 20 kHz tests.

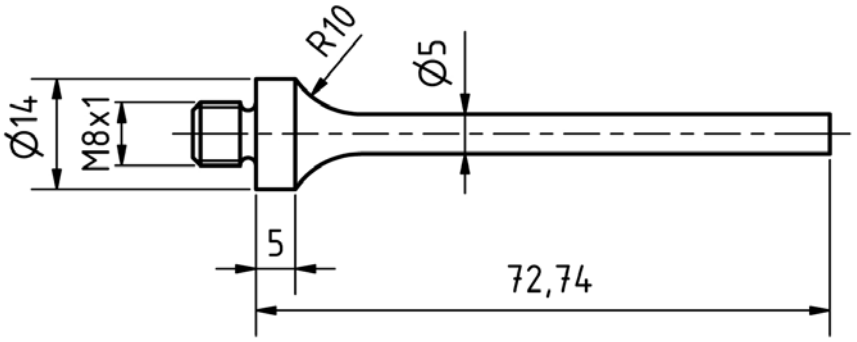

FIGURE 2.4: Specimen Shape for 20 kHz thermoelectric measurement of plastic strain amplitude.

2.3 Specimen Preparation

2.3.1 Surface Preparation

All specimens were ground after machining. Grinding was performed using an elastic grinding disc (Type 150-W) until no machining marks were visible at the specimen surface. The ground specimens were then heat treated and subsequently electrolytically polished.

The electrolyte used consists of 70 % phosphorous acid (with 75 % H_3PO_4) and 30 % demineralised water. The polishing procedure is as follows:

- 2 min electrolytic polishing
- rinsing in water
- cleaning with isopropyl
- 10 min electrolytic polishing
- rinsing in water
- rinsing with isopropyl
- drying with compressed air

Every 30 seconds, the quality of the electrolytic polishing process is checked. The Voltage is kept constant at 1.25 V using a DC power supply (Hewlett-Packard 6259B DC power supply 0-10 V 0-50 A).

2.3.2 Heat Treatment

The heat treatment was conducted in a furnace in high vacuum. The vacuum was typically $5 \cdot 10^{-5}$ mbar. A Pfeiffer vacuum system (HiCUBE) was used together with a GERO furnace (Type F). The heat treatment was performed as follows:

- heating from room temperature to 680 °C using a ramp of 300 °C/h
- holding for 25 min
- furnace cooling with a maximal rate of 300 °C/h until room temperature

Each batch consisted of four specimens of the same size. The specimens used for the thermoelectric measurements of the plastic strain amplitude were heat treated in batches of two.

Some of the specimens used for the 20 Hz tests were bent accidently while preparation. These specimens were straightened and stress relief annealed. The annealing was conducted as follows:

- heating from room temperature to 200 °C using a ramp of 300 °C/h
- holding for 2 h
- furnace cooling with a maximal rate of 300 °C/h until room temperature

2.4 Testing Equipment

A servohydraulic testing machine (Schenck PSA 40 controlled via the software Test and Motion by doli) operating at a pressure of 180 bar was used for tests at 20 Hz. It was operated in load control using a 40 kN load cell. PID parameters and sensor data are listed in the Appendix C.

Ultrasonic fatigue testing equipment (developed at BOKU) operating in the range of 18 to 21.5 kHz was used for tests at approximately 20 kHz. The exact testing frequency is depending on the resonance frequency of the system used (ultrasonic converter, horn and specimen), and can vary throughout the test, as for example a crack, changes in the specimen temperature and cyclic hardening or softening change the resonance frequency. The test is automatically stopped whenever the resonance frequency decreases more than 300 Hz from its initial value or the vibration amplitude cannot reach 85 % of the set value within 100 ms. It is also possible to set a smaller frequency bound. But this is not useful here as the frequency undergoes large changes due to cyclic hardening during the training procedure anyway.

The fatigue testing equipment operates in closed loop control [39]. The test is controlled by the ultrasonic fatigue test generator. It controls the vibration amplitude and the resonance frequency with an accuracy of $\pm 1\%$ and ± 1Hz, respectively [40].

The vibration is actuated by a piezoelectric transducer and magnified by a titanium horn. The vibration amplitude is maximum at the ends of the specimen and has a vibration node at the centre of the specimen. The vibration amplitude is measured with a vibration gauge placed at the horn close to the specimen end. The vibration gauge works by induction and the output signal is proportional to the actuation. Assuming that the specimen vibrates in the linear elastic regime, the feedback signal of the vibration gauge is proportional to the strain at the centre of the specimen [39, 40].

At the beginning of every test series, the system is calibrated using a strain gauge conditioner to measure strains at ultrasonic frequencies. At the centre of the specimen where the strain is maximum two strain gauges (with an area of 1 mm^2 each) are applied. The total strain amplitude is measured and averaged. A linear relationship between nominal amplitude and effective total strain amplitude is assumed. Based on this assumption, the nominal stress amplitude can be calculated for every vibration amplitude set using Hooke's law [11, 39].

The fatigue testing equipment facilitates not only continuous loading but also pulsed operation. The pulse length can be set from 1 to 990 ms interrupted by pauses of 1 to 9900 ms. The specimen is also cooled by compressed air, and to prevent specimen

heating, a proper pulse-pause relation has to be chosen. Incorrect operation can cause severe specimen heating leading to early failure.

All cycles that reach more than 85 % of the set amplitude are counted and the number of cycles N is displayed at the fatigue test generator. Up to four power-amplifiers can be used within the ultrasonic fatigue testing equipment. If the number of amplifiers used is reduced, the load at a certain amplitude set is reduced. For the current tests only two amplifiers were used.

Stress cannot be measured directly whenever ultrasonic fatigue testing technique is used, but if the material is tested within its elastic range, the stress can be calculated from the strain measured using Hooke's law. In the present tests, the strain was only measured while calibration based on the experience of former work [19]. A linear relationship between nominal amplitude and strain was assumed (the results presented in Chapter 2.5.3 verify this assumption). The nominal stress amplitude is therefore calculated from the calibration data.

2.5 Test Setup

All tests were conducted at room temperature under controlled laboratory conditions (T=23 °C, humidity: 50 %).

For fatigue tests at 20 Hz, servohydraulic testing equipment (Schenck PSA40 with doli EDC 580 controller and doli Test and Motion software) was used and specimens were mounted by collet chucks. Tests were conducted in load control until failure or were stopped after $5 \cdot 10^7$ cycles. A training procedure was chosen before testing in accordance with former tests [37]. The specimens were ramp loaded beginning at 10 MPa in steps of 1 MPa and a step length of 300 cycles. After ramp loading, tests were conducted with a constant load amplitude. Number of cycles to failure N_f were counted from the end of ramp loading until final failure.

For the 20 kHz tests, an ultrasonic fatigue testing equipment was used. The specimen is screwed directly into the horn and vibrates in free resonance. Pulse-pause loading was used to prevent self-heating of the specimen while testing. Additionally, specimens were cooled by compressed air. The automatic stop of the tests (see Chapter 2.4) was used as failure criterion. A training procedure was chosen in accordance with former tests [19, 38]. The training procedure started at a nominal stress amplitude of 10 MPa and was increased in steps of 1 MPa with a step length of $2.1 \cdot 10^4$ cycles. Specimens were

tested until the ultrasonic fatigue testing equipment stopped automatically or they were considered run out specimens if they survived 10^9 cycles[1].

To ensure comparability of the tests, all specimens have to be mounted without applying any stresses in the gauge section. This can be easily ensured for ultrasonic fatigue tests at fully reversed loading, since specimens are only mounted at one end. They are screwed into the ultrasonic horn, and if force is only applied at the upper part near the thread, no stresses act upon the specimen's gauge section. But mounting specimens into the load frame of a servohydraulic testing device is more complicated. It has to be ensured that no momentum and no force is applied. As the Schenck PSA40's piston is floating in oil, no momentum can be transmitted. Specimens are mounted first into the lower collet chuck. To mount the specimen in the upper collet chuck the force is kept zero by the controller. To check whether this procedure is permissible the specimen surface was investigated using light optical microscopy before and after mounting (see Chapter 3.4 and Appendix E, Figures E.1 and E.2 for details). As no slip markings were observed, the mounting procedure was considered permissible.

2.5.1 Plastic Strain Amplitude 20 Hz

Preliminary tests to record test data directly were preformed using HBM Spider 8 and Test and Motion software. Spider 8 was connected via LPT port (in EPP mode) to the computer. The Test and Motion software is able to read the data directly from Spider 8 and record it together with the (machine)sensor data (here: force, piston position, time, cycles). To verify correct data recording, a step response test was performed in load control. Strain gauges in half bridge circuit were applied to an hourglass shaped specimen. The load was changed from 0 to 500 N with a velocity of 5000 N/s. The data from the load cell (directly via EDC 580) and the data form the strain gauges (via Spider 8) were recorded using Test and Motion. The data was analysed thereon and no time delay between recording via Spider 8 and EDC 580 was found. Investigating the step response, it was found that the data acquisition rate of 500 Hz is not achieved when using Spider 8. The load cell data is recorded correctly with 500 Hz. Data from Spider 8 is recorded with 500 Hz also but there are always three identical data points recorded. Figure 2.5 shows the data recorded. The load cell signal is marked by down-pointing triangles. The signal recorded by Spider 8 is marked by circles. Only the first of these three data points (marked by a filled symbol) corresponds to a real value. The other two have to be filtered.

[1] Two specimens were cycled up to approximately $3 \cdot 10^{10}$ cycles but did not fail.

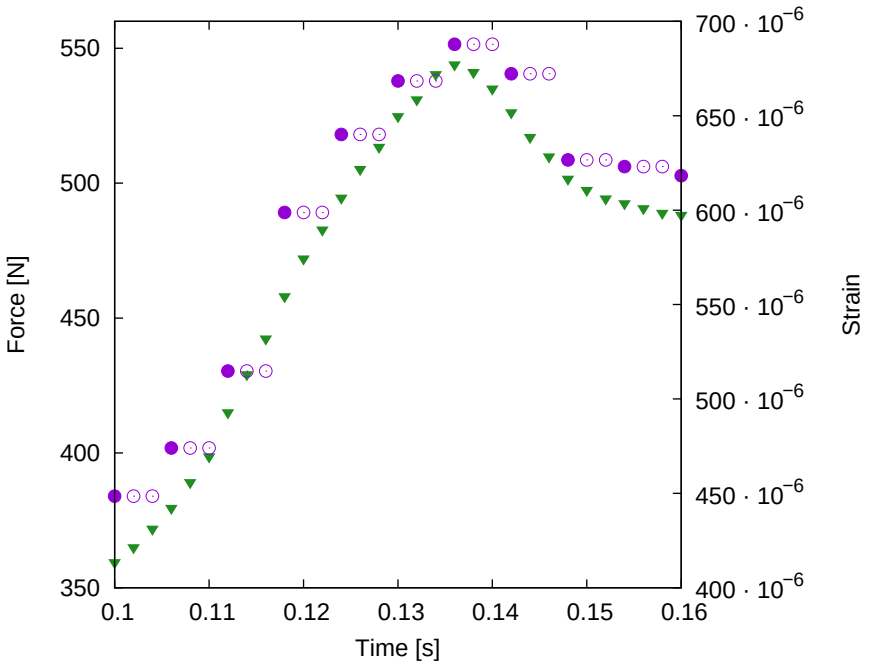

FIGURE 2.5: Datarecording Spider 8 (represented by circles) compared to recorded load cell signal (represented by triangles). Data points corresponding to real values are marked by filled symbols.

If a measurement does not demand very high resolution, Spider 8 can be used if these identical data points are removed. But it is not possible to use Spider 8 for recording hysteresis loops at 20 Hz. The 20 Hz sine has to be scanned with a sufficient data acquisition rate to be able to plot the actual hysteresis loop's shape. 500 Hz is sufficient to scan a 20 Hz sine but the reduced acquisition rate with Spider 8 gives insufficient data to plot hysteresis loops. As the influence of cyclic frequency is investigated here lowering the testing frequency (to achieve acceptable data) is no option.

To record the data correctly, a doli sensor plug was used. The strain can be recorded directly via EDC 580 together with force, piston position, time and cycles. The sensor plug has an EEPROM to store the sensor data. The configuration of the sensor's EEPROM is listed in the Appendix C.

For the half bridge circuit, one strain gauge is applied in the centre of the specimen. The other one is applied perpendicular at the end of the hourglass section, where no strain is expected, for temperature compensation.

The Test and Motion software has some limitations regarding data acquisition. It is not possible to save all cycles. The first cycle is not saved. From cycle two to eleven, every cycle is saved. Then every tenth (hundredth, thousandth, ...) cycle is saved.

2.5.1.1 Measurement while Training

Consistent with present and previous measurements [20, 38] at 20 kHz, the plastic strain amplitude was measured every fifth load step. Beginning with a stress amplitude of 10 MPa, the load was increased in steps of 1 MPa after a certain number of cycles. The step length of every step where the plastic strain amplitude was measured was five times the step length used in the SN-tests, namely 1500 cycles[2]. For every other step, the step length was the same as in the SN-tests, namely 300 cycles. As the data recording is limited by Test and Motion, fifteen blocks of a 100 cycles length were added to be able to record more data.

Following the measurement, the recorded data was evaluated by a phython program. It is listed in the Appendix D.1. The results are presented in Chapter 3.2.1.

2.5.1.2 Measurement while SN-Testing

To obtain data on the evolution of the plastic strain amplitude while SN-testing, the plastic strain amplitude was measured for the highest and lowest stress level tested. The training procedure was identical with the other SN-tests. Data were recorded automatically by the Test and Motion software.

Following the measurement, the recorded data were evaluated by a phython program. It is listed in the Appendix D.2 and D.3. The results are presented in Chapter 3.2.2.

2.5.1.3 Data Evaluation

The data recorded during the tests are evaluated using python programs. They can be found in the Appendix D. To calculate the plastic strain amplitude, the single hysteresis loops were interpreted according to Figure 1.1.

Depending on the connection of the strain gauges to the Sensor (one measuring the strain, one for temperature compensation), the signal has to be multiplied with -1. The strain's sign in a tension half cycle has to be positive.

The first 21 cycles of every block are discarded when evaluating the data. The load amplitude is increased from zero during these cycles and has not reached the nominal value.

[2] In [20] the step length was 5000 cycles for the plastic strain measurement, but based on knowledge of the obtained plastic strains, consistency with the 20 kHz tests performed (present tests as well as in [38]) was considered more important for this study.

2.5.2 Plastic Strain Amplitude 20 kHz

The plastic strain amplitude at 20 kHz was measured thermoelectrically similar to [41]. With this method, it is possible to measure the average plastic strain amplitude over a pulse of N cycles.

The measurement is performed as described in [19, 38]. The plastic strain amplitude $\Delta\varepsilon_{pl}/2$ was measured every 5 MPa. Beginning with a nominal stress amplitude of 10 MPa the load was increased in steps of 1 MPa. The step length of every step where the plastic strain amplitude was measured was five times the step length used in the SN-tests, namely 10^5 cycles.

A k-type thermocouple with a welding contact with a thickness of 0.1 mm and threads with a diameter of 75 µm is used. The welding contact is mounted to the specimen by adhesive tape. To measure the temperature change caused by one pulse, an Agilent 34410A 6 1/2 digit multimeter is used. It has higher accuracy than the FLUKE 45 that was used in previous measurements. For details on the specimen shape used see Chapter 2.2, Figure 2.4.

The dissipated energy per cycle $\Delta W/\ N$ can be linked to the plastic strain amplitude $\Delta\varepsilon_{pl}/2$ as follows:

The dissipated energy per cycle $\Delta W/\ N$ is calculated using the heat capacity c, the mass m and the temperature change per cycle $\Delta T/N$

$$\frac{\Delta W}{N} = c \cdot m \cdot \frac{\Delta T}{N} = c \cdot \rho \cdot V \cdot \frac{\Delta T}{N} \tag{2.1}$$

The hysteresis loop's shape (see Figure 1.1) is approximated by an ellipse with area A. The area A corresponds to the dissipated energy per cycle $\Delta W/\ N$.

$$A = \Delta\varepsilon_{pl} \cdot \frac{\Delta\sigma}{2} \cdot \pi = \frac{\Delta W}{N} \tag{2.2}$$

Therefore the plastic strain can be calculated:

$$\Delta\varepsilon_{pl} = \frac{1}{2} \cdot \frac{c \cdot \rho \cdot V \cdot \Delta T}{\pi \cdot \frac{\Delta\sigma}{2} \cdot N} \tag{2.3}$$

Heat capacity c and density ρ at room temperature for Cu-ETP [42]:

$c = 0.386\,\mathrm{J\,K/g}$
$\rho = 8.93\,\mathrm{g/cm}$

2.5.3 Linearity of 20 kHz Measurement

To verify the assumption of a linear relationship between nominal stress amplitude and strain amplitude, an additional measurement was performed. Using an hourglass shaped specimen (namely U18), the total strain amplitude was measured up to a nominal stress amplitude of 110 MPa while training. The measurement started at a nominal stress amplitude of 11 MPa. The load was increased in steps of 1 MPa with a step length of approximately 19000 cycles. In Figure 2.6 the nominal stress amplitude is plotted over the total strain amplitude measured. No deviation from the expected linear behaviour was found within the range of the measurements performed (namely up to 100 MPa). At higher strain levels the relationship is not linear any more.

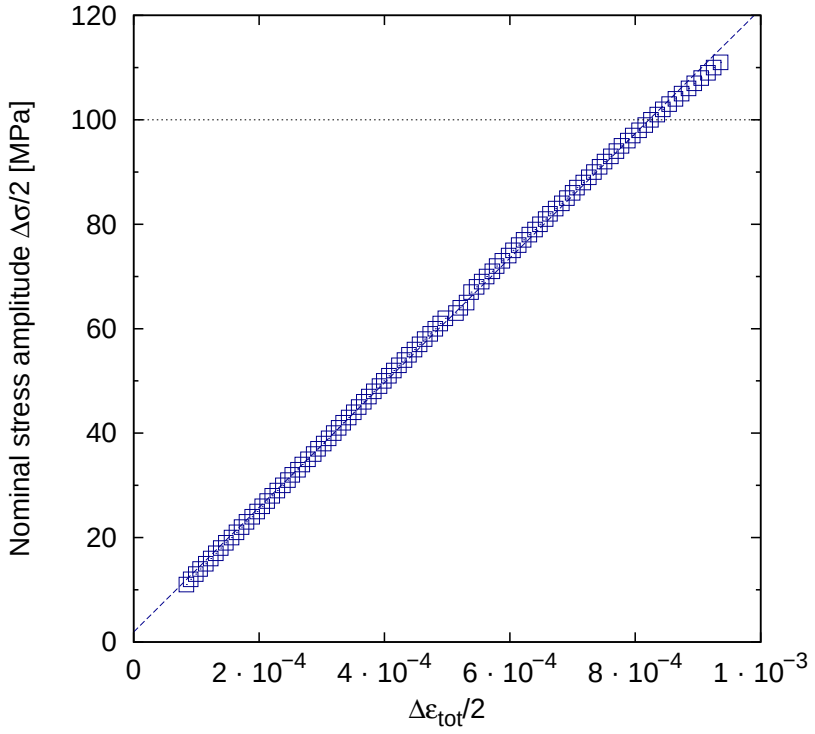

FIGURE 2.6: Linearity of 20 kHz measurement.

Chapter 3

Results

3.1 SN-Tests

3.1.1 20 Hz

The SN-tests' results at 20 Hz are shown in Figure 3.1. Failures are marked by open symbols. If a specimen survives $5 \cdot 10^7$ cycles, it is considered a run-out specimen and marked by filled symbols. The 10, 50 and 90 % fracture probability are calculated according to Chapter 1.9 by fitting the data of all stress levels that did show no run-outs. In Figure 3.1 the 10, 50 and 90 % fracture probability are represented by a dashed, solid and dotted line respectively.

3.1.2 20 kHz

The test results at 20 kHz are shown in Figure 3.2 in an SN-diagram. Failures are marked by open symbols. Specimens surviving 10^9 cycles are considered run-out specimens and marked by filled symbols. Two specimens were tested up to $3 \cdot 10^{10}$ cycles and did not fail. The 10, 50 and 90 % fracture probability are calculated according to Chapter 1.9 by fitting the data of all stress levels that did show no run-outs. In Figure 3.2 the 10, 50 and 90 % fracture probability are represented by a dashed, solid and dotted line respectively.

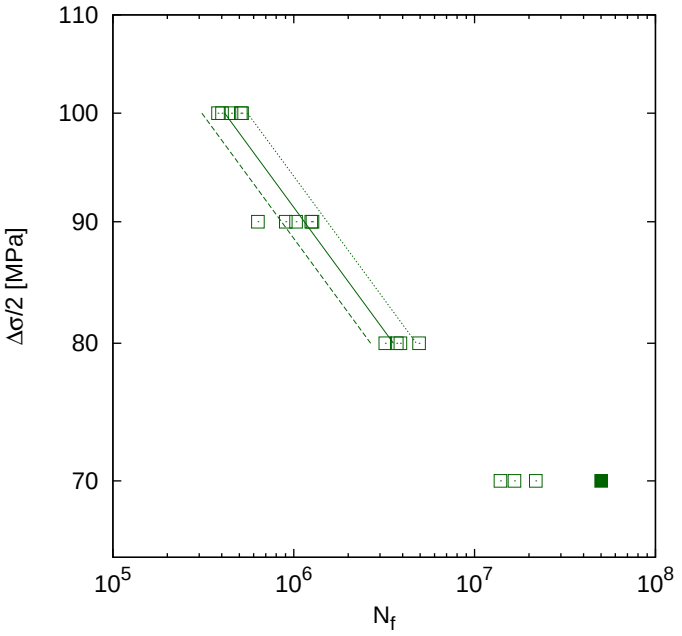

FIGURE 3.1: 20 Hz results. Failures are marked by open symbols; run-outs by filled symbols. The dashed, solid and dotted line represent the 10, 50 and 90 % fracture probability respectively.

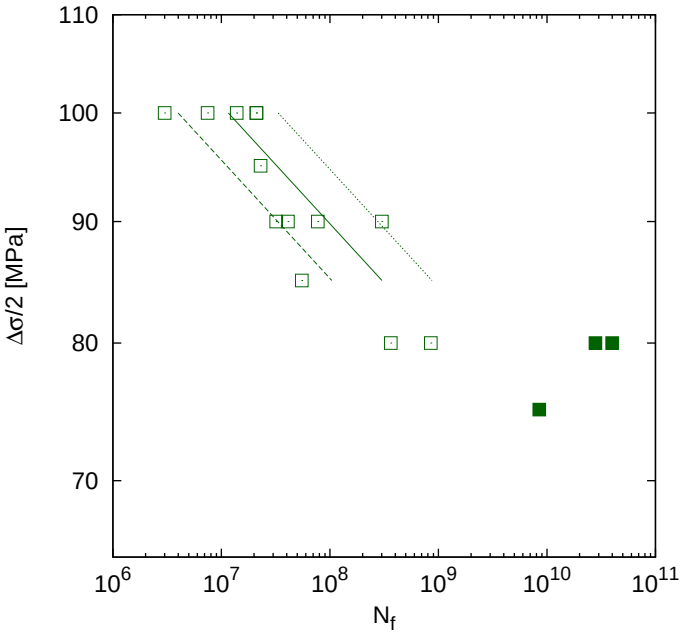

FIGURE 3.2: 20 kHz results. Failures are marked by open symbols; run-outs by filled symbols. The dashed, solid and dotted line represent the 10, 50 and 90 % fracture probability respectively.

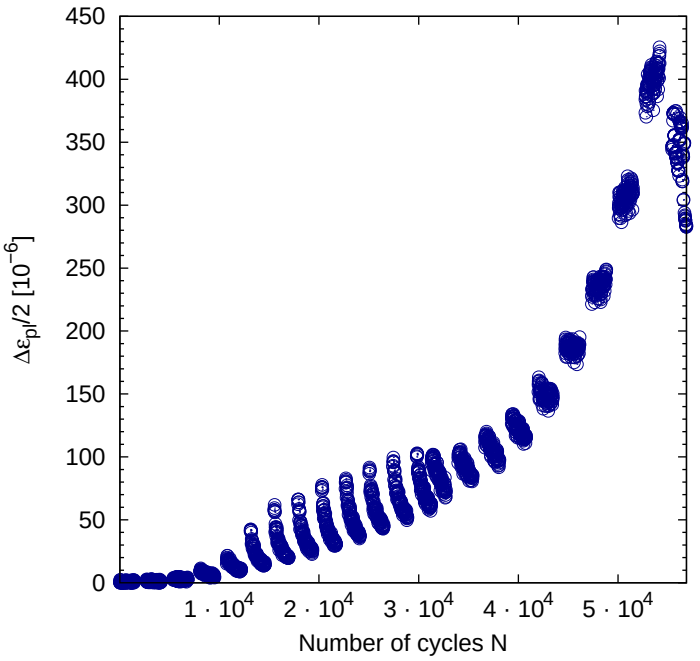

FIGURE 3.3: Plastic strain amplitude 20 Hz.

3.2 Plastic Strain Amplitude

3.2.1 Plastic Strain Amplitude while Training at 20 Hz

The results of the plastic strain measurement while training are shown in Figure 3.3. Beginning with 10 MPa, the plastic strain at every fifth load level is plotted. The plastic strain amplitude is calculated from the single hysteresis loops measured. Details on the test setup and data evaluation are listed in Chapter 2.5.1.1 and Appendix D.1. Figures 3.4 to 3.6 are details of Figure 3.3 with the aim to give a better insight, as Figure 3.3 is a very general overview over the measurement.

For very low load levels (10, 15 and 20 MPa) no cyclic hardening or softening is visible. Figure 3.4 shows the data obtained in detail. The plastic strain amplitude is constant with a mean plastic strain amplitude of $7 \cdot 10^{-7}$, $1.3 \cdot 10^{-6}$ and $2.7 \cdot 10^{-6}$ respectively. For all other load levels the plastic strain amplitude is not constant. At most load levels it changes significantly while training.

No distinguished cyclic hardening can be found for load levels below 35 MPa. In the range of 35 to 75 MPa strong cyclic hardening is visible. Figure 3.5 shows data of three load levels in this range in detail. In the range between 80 and 95 MPa cyclic hardening is less pronounced. At 100 MPa no cyclic hardening is visible. At 105 and 110 MPa little cyclic softening is visible. Figure 3.6 shows the data in detail. At the highest load levels (115 and 120 MPa, last two block in Figure 3.3) the measurement using strain gauges is

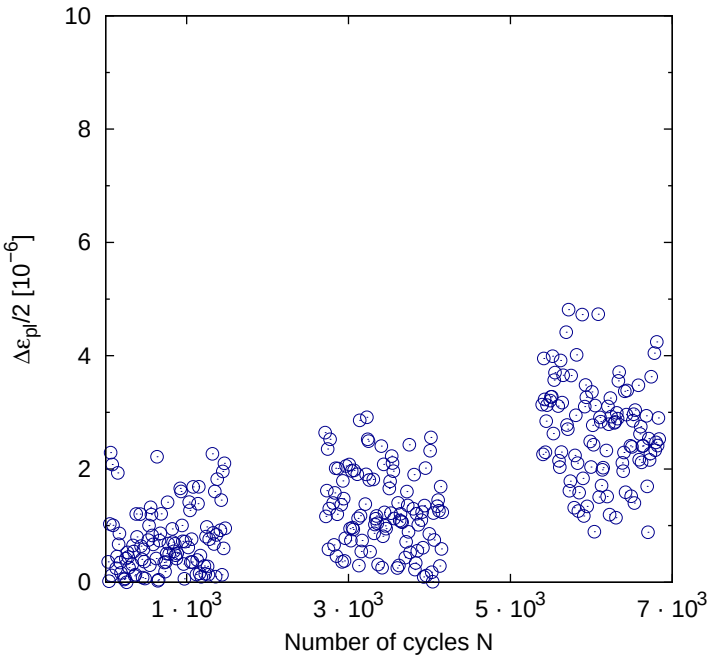

FIGURE 3.4: Plastic strain amplitude at 20 Hz for 10 MPa (left block), 15 MPa (middle block), 20 MPa (right block).

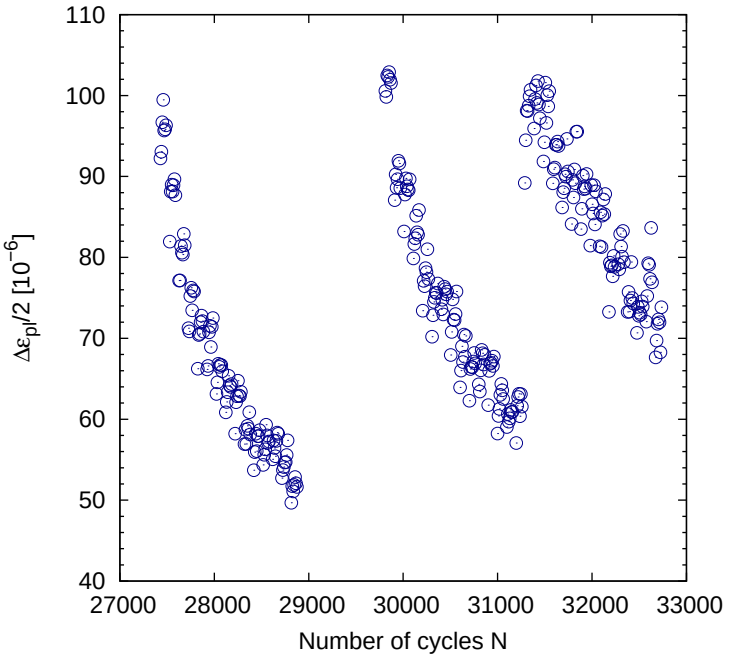

FIGURE 3.5: Plastic strain amplitude at 20 Hz for 65 MPa (left block), 70 MPa (middle block) and 75 MPa (right block).

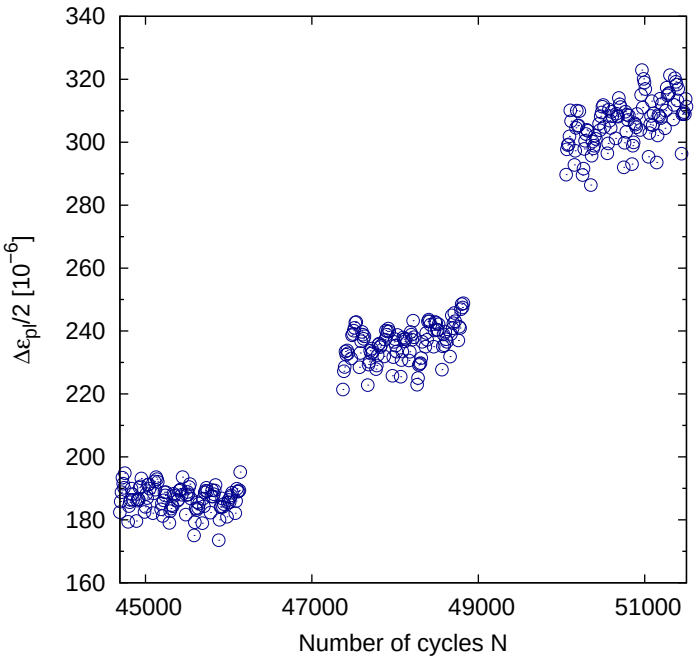

FIGURE 3.6: Plastic strain amplitude at 20 Hz for 100 MPa (left block), 105 MPa (middle block), 110 MPa (right block).

not useful as the limit of the strain gauges is already reached. At such high load levels anyway no SN-tests were performed. (The highest load level tested was 100 MPa.)

Analysing hysteresis loops, it has to be noted that in general the hysteresis loops are not closed. A tensile strain is accumulated.

In general it is noted that saturation is not reached within the load steps measured. The step length in the training procedure applied in SN-tests is only one fifth of the step length used for this measurement. Therefore, it can be stated that saturation is not reached while training.

3.2.2 Plastic Strain Amplitude while Testing at 20 Hz

The plastic strain amplitude was measured while testing at the highest and lowest load level tested, namely 70 and 100 MPa. Details on test setup and data evaluation are listed in Chapter 2.5.1.2 and Appendix D.2 and D.3 respectively.

Figure 3.7 shows the results for the highest load level tested (100 MPa). While the plastic strain amplitude can be considered constant until $3 \cdot 10^3$ cycles, distinct cyclic softening occurs afterwards. Note that the last data point was recorded at $5 \cdot 10^5$ cycles. The specimen failed at $5.1 \cdot 10^5$ cycles.

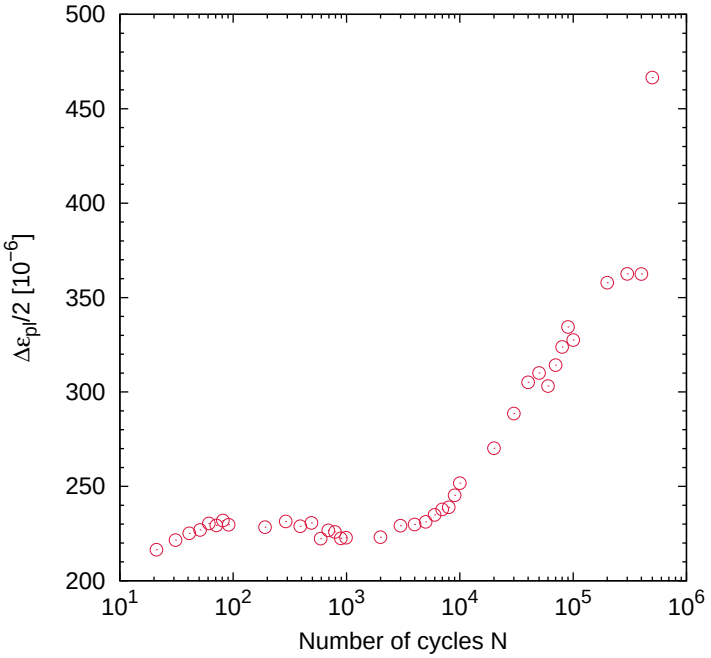

FIGURE 3.7: Plastic strain amplitude measured while SN-testing at 100 MPa.

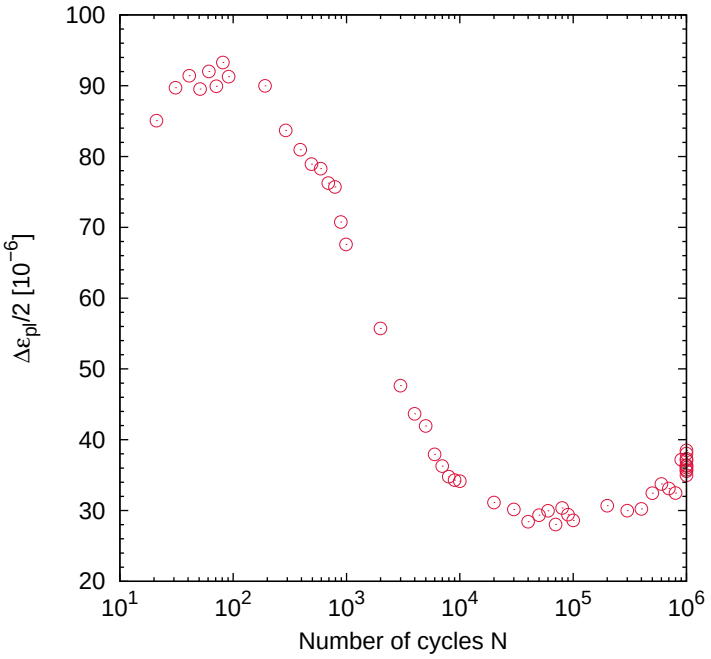

FIGURE 3.8: Plastic strain amplitude measured while SN-testing at 70 MPa.

Figure 3.8 shows the results for the lowest load level tested (70 MPa). It is noted that this specific specimen did not fail until $5 \cdot 10^7$ cycles while all other specimens tested at this load levels did fail in the range of $1.3 \cdot 10^7$ to $2.2 \cdot 10^7$ cycles. Also the data recording, which is limited by the test and motion software, did not work at high numbers of cycles. Nevertheless, the results show cyclic hardening up to $2 \cdot 10^4$ cycles followed by saturation with an almost constant plastic strain amplitude.

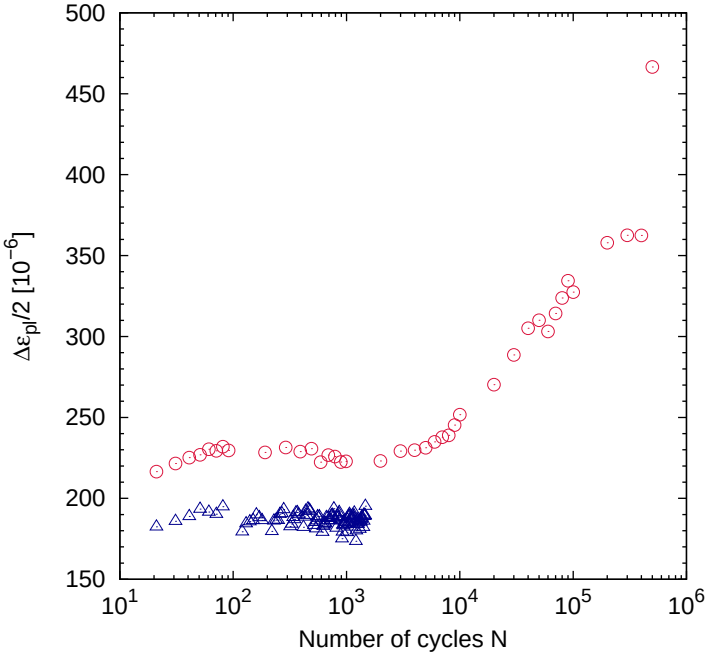

FIGURE 3.9: Comparison of plastic strain amplitude measurements while training (represented by triangles) and while SN-testing at 100 MPa (represented by circles).

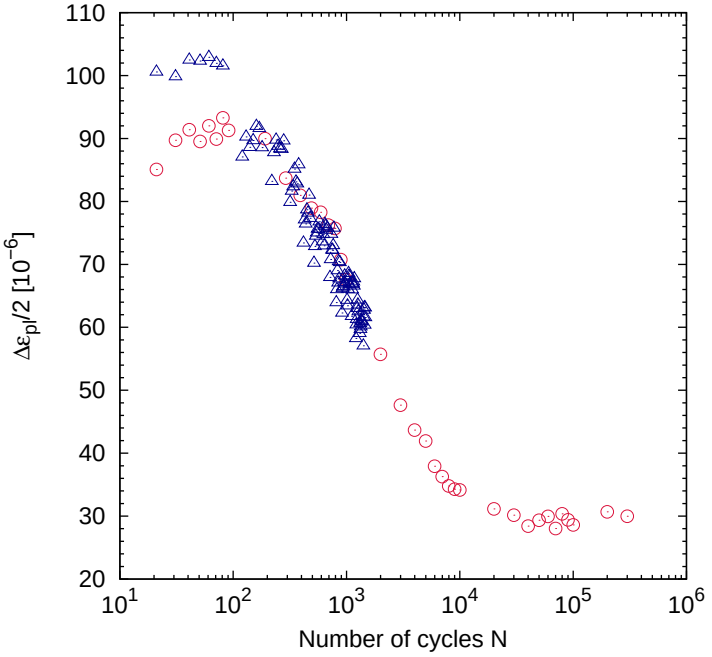

FIGURE 3.10: Comparison of plastic strain amplitude measurements while training (represented by triangles) and while SN-testing at 70 MPa (represented by circles).

Figures 3.9 and 3.10 compare the data obtained while training (represented by triangles) with the measurement while SN-testing (represented by circles). In general good accordance is found. The slightly lower plastic strain amplitude measured while training at 100 MPa (Figure 3.9) is likely to result from the differences in the applied training procedure. In the measurement during training, higher numbers of cycles are already achieved when the 100 MPa load level is reached, as the step length of every fifth step was five times the step length used in the measurement while SN-testing. Note that pronounced cyclic hardening occurred especially in the range of 35 to 95 MPa.

3.2.3 Plastic Strain Amplitude 20 kHz

The plastic strain was measured thermoelectrically. Details are given in Chapter 2.5.2. The measurement could not be performed in the whole range of nominal stress amplitudes used as the frequency change exceeded the ultrasonic testing equipment's limits. Therefore, the measurement was limited to a nominal stress amplitude below 77 MPa. The data obtained is compared in Figure 3.11 with data obtained by Stanzl-Tschegg et al. [19] in a similar measurement. The present data are represented by filled up-pointing triangles, whereas formerly obtainded data is represented by down-pointing open triangles. As the data obtained is very well comparable, no change is expected for higher nominal stress amplitudes either. Therefore the already existing data [19] was considered sufficient and no further measurement was performed.

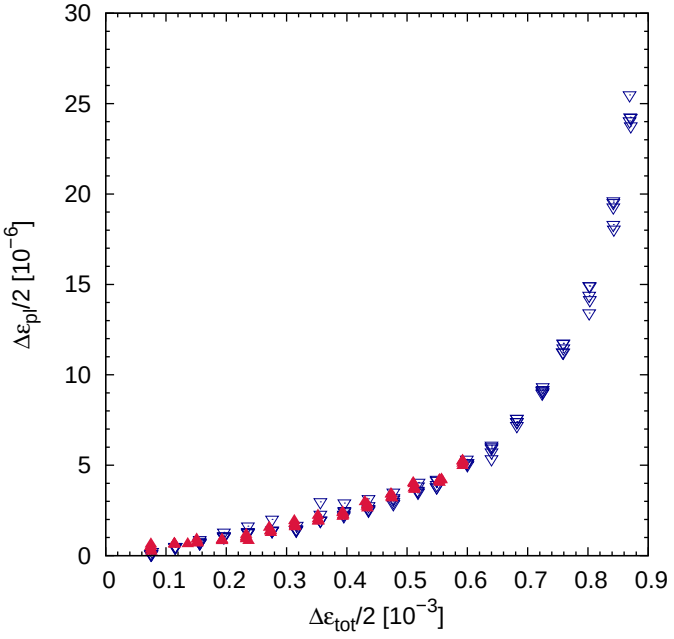

FIGURE 3.11: Comparison of the present plastic strain amplitude measurement (represented by up-pointing filled triangles) with [19] (represented by down-pointing open triangles).

3.3 Coffin-Manson Diagram

To plot the fatigue test results in to a Coffin-Manson diagram, the saturation value of the plastic strain amplitude for a given nominal stress amplitude is used.

For 20 kHz results, the plastic strain amplitude data obtained by former tests [19] was used. The saturation value was calculated as the mean value of the last two measurements at each nominal stress level. The Coffin-Manson diagram obtained is shown in Figure 3.12.

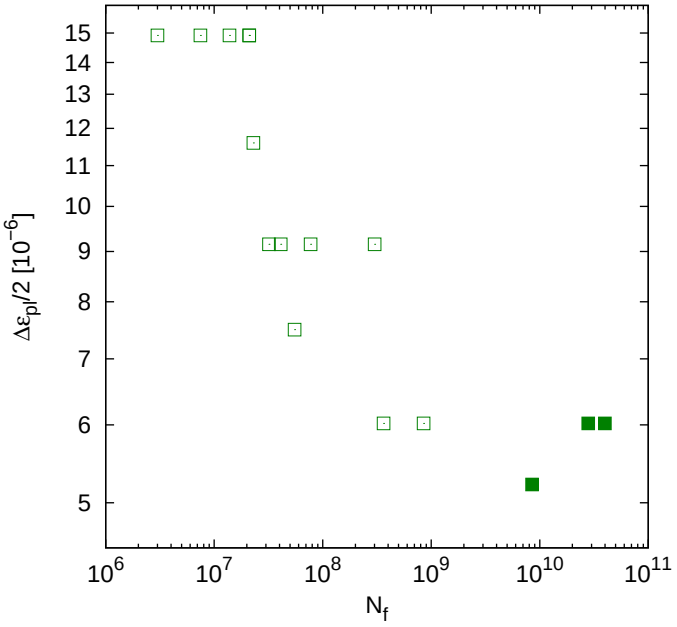

FIGURE 3.12: 20 kHz results transformed to a Coffin-Manson diagram. Failures are marked by open symbols; run-outs by filled symbols.

For 20 Hz results, the plastic strain amplitude data obtained while SN-testing was used, as saturation was not reached while training (for details see Chapter 3.2.1 and 3.2.2). Plastic strain amplitudes were measured at the highest and lowest stress level tested. The saturation values were calculated from the data obtained within these tests. For the lowest load level (namely 70 MPa, see Figure 3.8) saturation was reached after $2 \cdot 10^4$ cycles. The mean value of all valid data points with $N > 2 \cdot 10^4$ cycles was taken as saturation value of the plastic strain amplitude (namely 11 data points). For the highest load level (namely 100 MPa, see Figure 3.7) no initial cyclic hardening was observed. The first three data points (Figure 3.7) where the plastic strain amplitude is increasing slightly were skipped. The following data points up to $3 \cdot 10^3$ cycles were used to calculate the plastic strain amplitude (17 data points). The plastic strain amplitudes of the other load levels were estimated by these values using an exponential fit. The Coffin-Manson diagram obtained is shown in Figure 3.13.

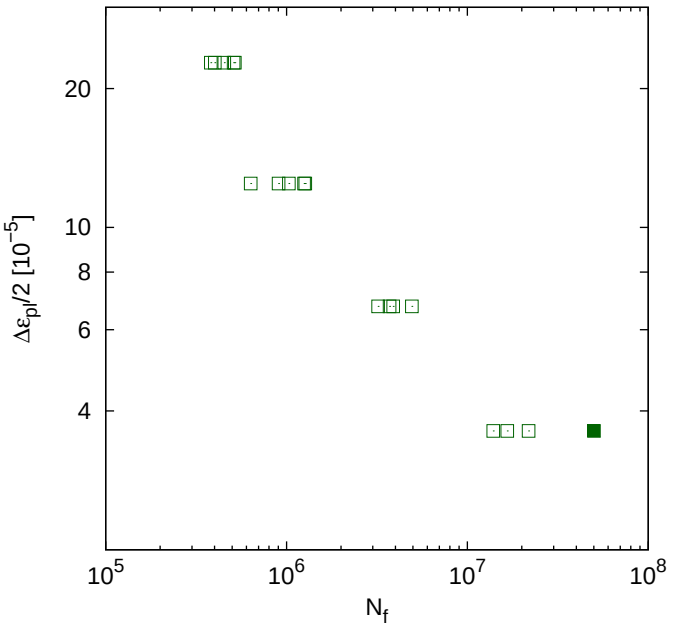

FIGURE 3.13: 20 Hz results transformed to a Coffin-Manson diagram. Failures are marked by open symbols; run-outs by filled symbols.

3.4 Evolution of Slip Markings

The evolution of slip markings was investigated. SN-tests at the highest load level (nominal stress amplitude 100 MPa) were repeatedly interrupted and the specimens were investigated using a light optical microscope (Olympus BX 51). The specimen surface in the gauge length was divided into four segments. Images were taken at the same position every time. Details are listed in the Appendix E.

Slip markings appeared for both testing frequencies already during the training procedure. These slip markings were limited to some grains only. For 20 Hz the number of very pronounced slip markings is higher at that initial stage of testing (after the training procedure) compared to 20 kHz. Still, also some very pronounced slip markings are visible when tested at 20 kHz. The amount of slip markings increases for both testing frequencies with number of cycles applied. Also the number of grains covered by slip markings increases with number of cycles. For 20 Hz almost all grains are covered by slip markings before failure. Concerning 20 kHz, the number of grains that are not covered by slip markings is significantly higher.

The appearance of slip markings differs clearly for 20 Hz and 20 kHz.

Using light optical microscopy, three different forms of slip markings could be identified when tested at 20 kHz:

- Isolated slip bands which often appeared already during the training procedure and become more pronounced with number of cycles accumulated were observed in some grains.
- A number of parallel slip bands increasing in number with number of cycles applied were observed. The grain's coverage by these parallel slip band also is increased with number of cycles.
- Very faint slip markings that manifest in a weak surface roughening were observed solely at 20 kHz. This surface roughening appears by a different colour compared to areas without slip markings when observed with a light optical microscope. The area covered by this surface roughening is increased with numbers of cycles. In some grains these very small slip markings appeared exclusively while in others they appear together with parallel slip bands.

Pronounced parallel slip bands covering the grain are the predominant slip marking observed at 20 Hz. In very few grains, isolated slip bands were observed. The surface roughening due to vague slip markings as observed at 20 kHz was not observed at 20 Hz.

At 20 Hz a crack already appeared at relatively low numbers of cycles. The crack growth rate increased with numbers of cycles throughout the test. No dominant crack was observed at 20 kHz[1]. Figure 3.14 shows the specimen surface after $5.67 \cdot 10^6$ cycles.

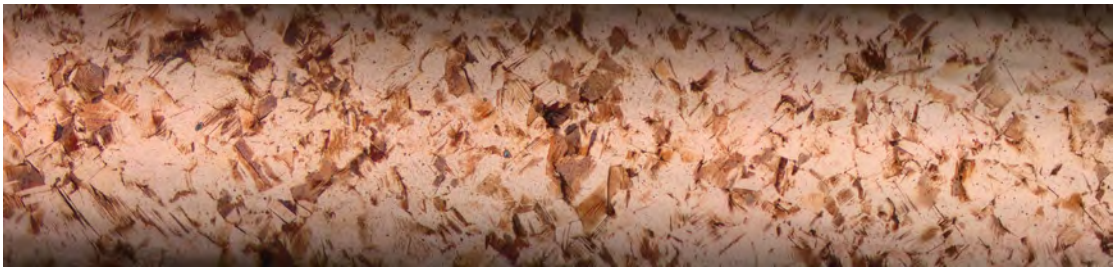

FIGURE 3.14: Overview of the specimen surface exhibiting slip markings at 20 kHz ($N = 5.67 \cdot 10^6$ cycles).

[1]Note that the specimen did not show fatigue failure. It was not possible to perform the test until failure as the specimen failed at the thread due to repeated mounting.

Chapter 4

Discussion

4.1 Influences

4.1.1 Influence of Test Control

In the range of small amplitudes where ultrasonic fatigue testing technique usually is applied, the plastic strain amplitude is only a rather small part of the total strain amplitude. Therefore, total strain controlled tests are nearly equivalent to stress controlled tests [43].

4.1.2 Influence of Test Setup

Stanzl-Tschegg et al. [19] suggest that the low plastic strain amplitudes they observed at ultrasonic frequencies are a consequence of the high testing frequency and the training procedure applied leading to a more pronounced hardening. This suggestion is in good accordance with Yan and Laird's [31] findings for copper single crystals. They found that using a Neumann loading mode (a linear increase of load with number of cycles) plays a significant role in causing a higher PSB nucleation stress. They conclude that the plastic strain amplitude during cyclic hardening has a stronger influence than the frequency of cycling (here either 2 or 34 Hz).

Additionally, Llanes and Laird [25] found a pronounced influence of ramp loading in the range of 70 to 98 MPa, when they compared tests with and without initial ramp loading. Polák et al. [43] performed stress controlled tests at 80 Hz with polycrystalline copper of 99.99 % purity. The specimens were not ramp loaded. The results are within the range of the present results. Only the highest stress level shows a significantly earlier failure.

This leads to the assumption that the ramp loading procedure has a more pronounced influence at higher load levels. This assumption is supported by the current measurements: Concerning the 20 Hz tests, a lower plastic strain amplitude was found when testing at the highest stress level (namely 100 MPa) if the number of cycles while training was increased (see Figure 3.9). At the lowest stress level (namely 70 MPa) no differences concerning the plastic strain amplitude were observed (see Figure 3.10). Details are described in Chapter 3.2.2.

It is noted that the step length of the training procedure for 20 Hz tests is significantly lower compared to 20 kHz tests, namely 300 cycles for the 20 Hz tests and $2 \cdot 10^4$ cycles for the 20 kHz tests.

Stanzl-Tschegg and Schönbauer [18] studied the influence of the training procedure's step-height comparing 5 MPa steps to 1 MPa steps. No influence on the SN-results was found, but an overshoot of the initial plastic strain amplitude with subsequent cyclic hardening was found for the 5 MPa steps, whereas no such overshoot was found when steps of 1 MPa where used.

4.1.3 Influence of Testing Frequency

Figure 4.1 and 4.2 show in an SN-diagram all present results. Figure 4.1 shows the clear shift towards higher numbers of cycles to failure at a comparable nominal stress amplitude. Figure 4.2 presents the data in a Coffin-Manson diagram. Details on the calculation of the Coffin-Manson diagram are listed in Chapter 3.3. The different plastic strain amplitudes for 20 Hz and 20 kHz tests at the same nominal cyclic stress amplitudes are significant.

As explained in Chapters 4.1.1 and 4.1.2, the influences of test control and test setup are expected to be rather small. Therefore, a strong influence of testing frequency is indicated by these results. As tests are not completely comparable concerning test setup and test control, 20 Hz tests in total strain control using an identical training procedure would give a deeper insight on the quantity of the frequency effect as all other influences are excluded.

In the present tests a significantly higher plastic strain amplitude was found for 20 Hz tests compared to 20 kHz tests (for details see Chapter 3.2). This finding is in good accordance with reports from literature: Yan et al. [31] found investigating copper single crystals using also ramp loading that a decrease of testing frequency (from 34 to 2 Hz) lead to an increase of plastic strain amplitude. Mayer and Laird [34] also found this effect for stress levels greater than 90 MPa comparing very low testing frequencies (in

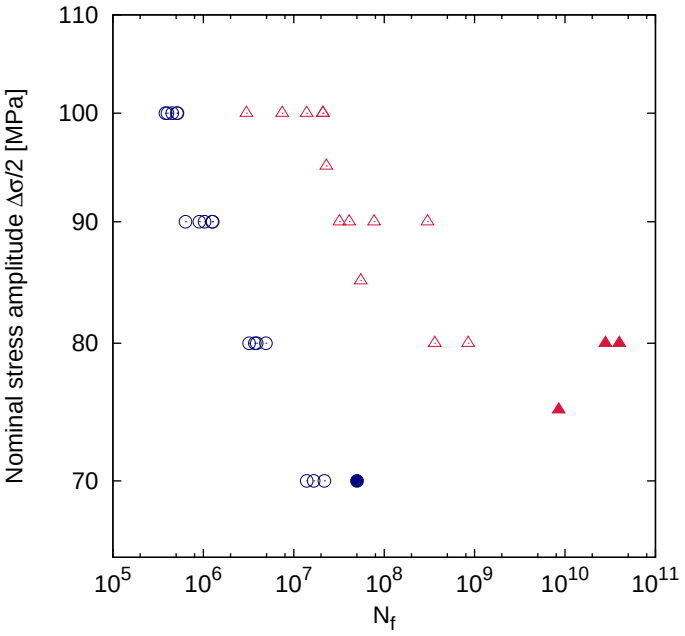

FIGURE 4.1: Comparison 20 Hz results (represented by circles) with 20 kHz results (represented by triangles) in an SN-diagram. Failures are marked by open symbols, whereas run-outs are marked by filled symbols.

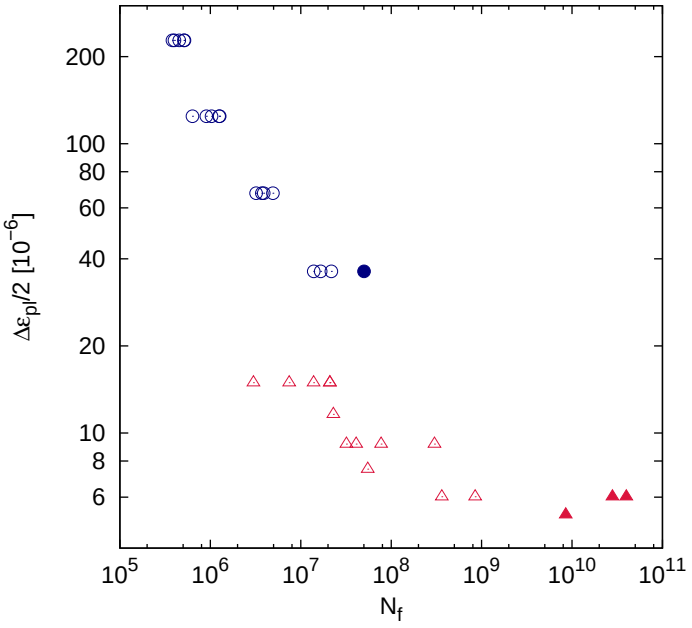

FIGURE 4.2: Comparison 20 Hz results (represented by circles) with 20 kHz results (represented by triangles) in a Coffin-Manson diagram. Failures are marked by open symbols, whereas run-outs are marked by filled symbols.

the range of 0.5 to 8 Hz). Stanzl-Tschegg and Schönbauer [20] also found this behaviour when comparing measurements at 20 Hz and 20 kHz.

No difference in the appearance of slip bands was detected by Awatani et al. between the 17.7 kHz tests and tests at conventional testing frequencies. Slip bands grew in length and width with increasing numbers of cycles. Also the dislocation structure found was very similar to the dislocation structure known for conventional test. Therefore they considered that the fatigue mechanism *"is almost (sic!) the same as that at lower frequencies"*. This observation may lead to the assumption that no frequency effect influences the fatigue behaviour, but a more detailed investigation shows that appearance and dislocation patterns of slip bands formed at 20 kHz differ significantly from PSBs observed at conventional testing frequencies. Stanzl-Tschegg and Schönbauer [20] performed TEM investigations of the dislocation structure of PSBs formed at ultrasonic testing frequencies. They found a precursor of the typical ladder-like structure PSBs show at conventional testing frequencies. Weidner et al. [21] investigated the dislocation structure of fatigued copper polycrystals in detail using scanning electron microscopy (SEM) together with focused ion beam (FIB) technology. Surface roughening and stage I crack initiation were found below the PSB threshold. It was found that cyclic slip occurred localized in slip lamellae which showed mainly an elongated cell structure. Only some slip lamellae were found which showed the classical ladder-like dislocation pattern. A frequency effect on the formation of the dislocation structure can therefore be expected.

In present tests no detailed investigation of slip markings and underlying dislocation structure was performed, but a general comparison of the evolution of slip markings was performed at a nominal stress amplitude of 100 MPa at 20 Hz and 20 kHz (details are listed in Chapter 3.4 and Appendix E). It was found that the appearance of slip markings differed depending on the testing frequency. Mason and Wood [36] also report observations on OFHC copper and alpha brass tested at ultrasonic frequencies and compare the slip bands with those formed at conventional testing frequencies. They state that at room temperature, slip at ultrasonic frequencies and strain amplitudes of 10^{-4} occurs in form of an isolated slip band which turns into a micro crack throughout the test. Results of present investigations on the evolution of slip markings (see Chapter 3.4) are not in agreement with these observations. It has been found that in a reasonable number of grains no slip markings were observed at 20 kHz, but groups of parallel slip bands and surface roughening have been observed as well as single slip bands. The observed slip markings at 20 kHz are in accordance with more recent reports from literature [20, 24]. Also the density of slip markings was higher for the lower testing frequency which is in good agreement with reports from Mayer and Laird [34] who also found this behaviour for testing frequencies in the range of 0.5 to 8 Hz.

4.2 Comparison with Literature

Present results are compared with Eichinger's results [37] in Figure 4.3. Present tests' failure are marked by open squares. Failure from [37] are marked by down-pointing open triangles. Run-outs are marked by filled symbols. The 50% fracture probability was calculated using all stress levels besides those including run-out specimens. It is marked by dashed lines.

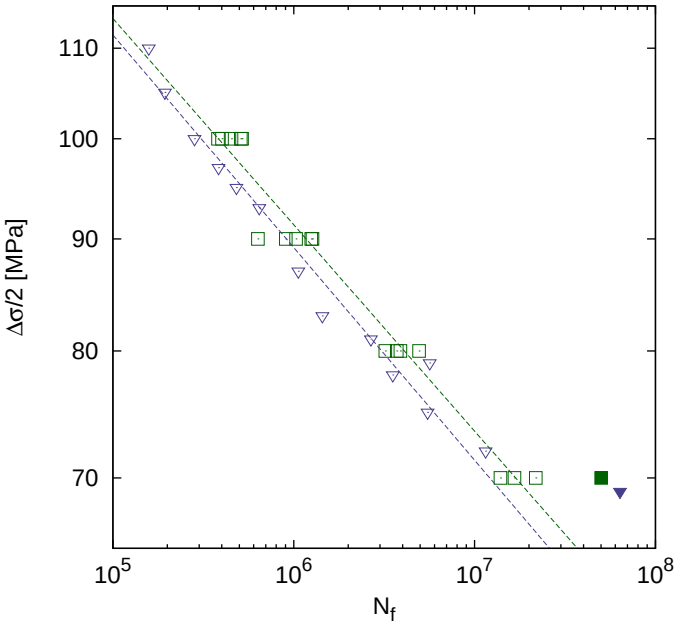

FIGURE 4.3: Comparison present 20 Hz results (represented by squares with [37] (represented by down-pointing triangles). Failures are marked by open symbols, whereas run-outs are marked by filled symbols.

The present results show a shift towards slightly higher numbers of cycles. When testing bent specimens, that were slightly deformed before mounting into the load frame, these results were generally similar (see Figure 4.4, bent specimens are represented by open up-pointing triangles). Failure occurred earlier and the results are in good accordance with [37]. Eichinger performed his measurements using similar specimen shape, heat treatment and testing procedure but at a different servohydraulic load frame. It can therefore be assumed that some damage happened to the specimens before testing or while mounting the specimens[1].

Marti et al. [35] have also published some results testing at 20 Hz among others. The testing material was OFHC copper and the mean grain size was 30 µm. Their results

[1]The piston's alignment has to be very precise to avoid unwanted momenta on the specimen. The piston's alignment on Schenck PSA40 has been checked before testing. In the meantime colleagues found out that the MTS' piston had been misaligned. As Eichinger used this load frames, the different results can therefore be very well explained by this fact.

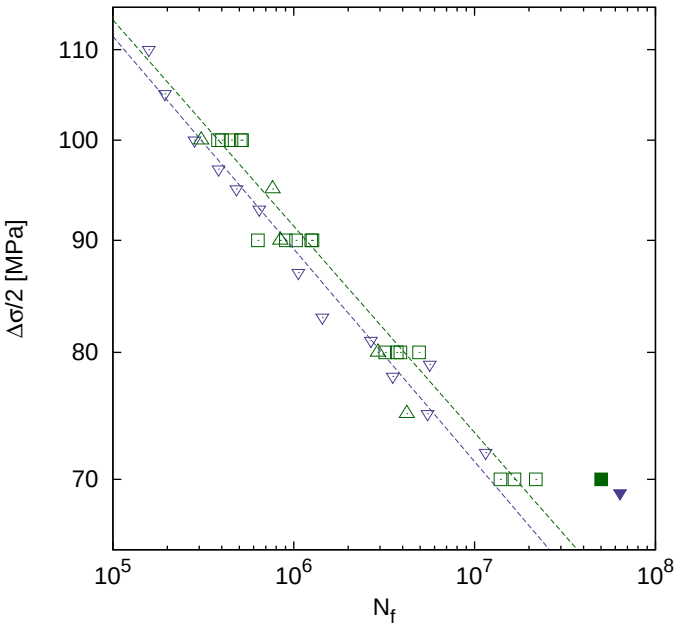

FIGURE 4.4: Comparison 20 Hz results including bent specimens (repesented by up-pointing triangles).

show broader scatter. As the testing procedure (including a possible training procedure) is not known, the results cannot be compared very well. But overall it can be said that their results are in agreement with the present and Eichinger's [37] results.

In Figure 4.5 and 4.6 a comparison of the present test with Stanzl-Tschegg and Schönbauer's results [18] is shown. Present tests' failure are marked by open squares. Failure from [18] are marked by up-pointing open triangles. Run-outs are marked by filled symbols. The present results exhibit failure at lower numbers of cycles. Failure also occurs at lower strain levels where tests reported in [18] did not show failure. Schönbauer also tested four specimens at a lower strain level ($\Delta\varepsilon_{tot}/2$ in the range of $6.94 \cdot 10^{-4}$ to $7.25 \cdot 10^{-4}$) which however, were not published [44]. All four specimens were stopped after at least $4 \cdot 10^8$ cycles. In the same range also four specimens were tested in the present tests. They all failed within $3 \cdot 10^7$ to $3 \cdot 10^8$ cycles.

The results plotted have an identical training procedure. The same material (Cu-ETP) was used for both tests but batches differed. The heat treatment was chosen so the same grain size was achieved though the exact heat treatment differs as a different furnace was used. The heat treatment formerly used was performed in low vacuum while specimens for present tests were heat treated in high vacuum ($5 \cdot 10^{-5}$ mbar). It is mentioned by Hessler et al. [45] that oxygen concentration while heat treatment has an influence on the fatigue behaviour of polycrystalline copper. The extent of this influence is unfortunately not reported. The present test's specimen shape was chosen

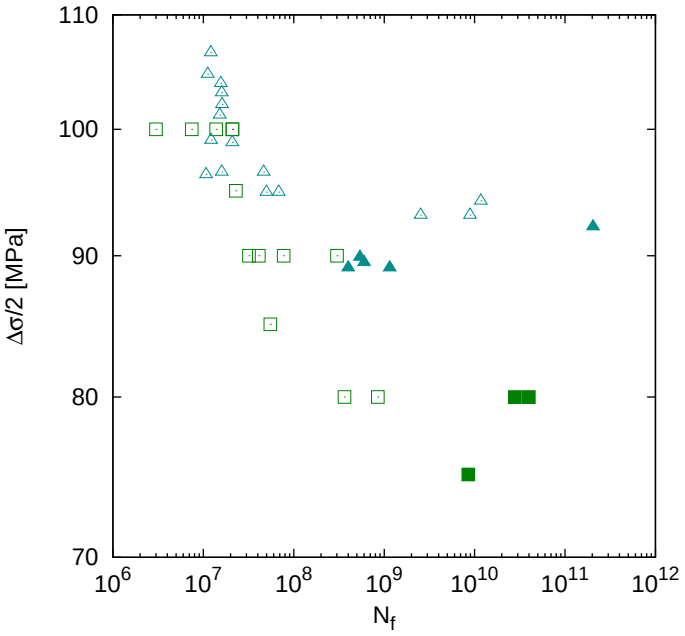

FIGURE 4.5: Comparison of present 20 kHz results (marked by squares) with [18] and [44] (represented by triangles) in an SN-diagram. Failures are marked by open symbols, whereas run-outs are marked by filled symbols.

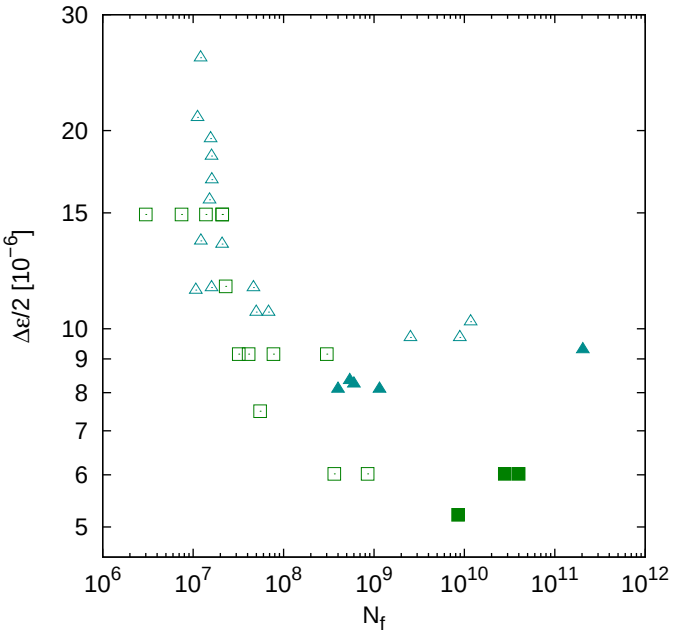

FIGURE 4.6: Comparison of present 20 kHz results (marked by squares) with [18] and [44] (represented by triangles) in a Coffin-Manson diagram. Failures are marked by open symbols, whereas run-outs are marked by filled symbols.

so the gauge volume is identical with former tests. The specimen shape differs as the maximum diameter of the specimens outside the gauge length was 8 mm in former tests (in contrast to 14 mm in the present test). Also these specimens were soldered into a mounting socket. Nevertheless the results of both tests should be well comparable. To investigate the cause of the different test results further, additional tests are needed.

Phung et al. [24] also performed ultrasonic fatigue tests. The material differs from the material in present and former [18–22] tests. The material used is OFHC copper (purity 99.95 %) with a mean grain size of 30 µm and an ultimate tensile strength of 230 MPa. Only data of 10 tests is reported and it is unknown if some kind of defined training procedure was used. The ultrasonic fatigue testing equipment used by Phung et al. does not allow pulse-pause loading. Therefore all tests were conducted with continuous loading. Phung et al. report that their results are in good agreement with the findings of Stanzl-Tschegg and Schönbauer [20]. Comparing Phung's results with the present test results, it is obvious that the present results show failure at lower number of cycles.

Comparing the 20 kHz results with Awatani et al.'s [9] results achieved at 17.7 kHz, a clear difference can be observed. Awatani et al. used commercially pure (99.95 %) copper for their tests. Heat treatment and grain size differ from the present tests. The grain size was in the range of 100 to 300 µm. Also the testing frequency differs slightly but it is in the range of 20 kHz. Another difference in test setup, is the cooling procedure used. While in present tests the specimens were subjected to intermittent loading and cooled by pulsed air, Awatani et al. loaded their specimens continuously and cooled them by a temperature controlled water flow. When comparing the results at 20 kHz to Awatani et al.'s results, it seems that their results are in good accordance with the current 20 kHz results for the highest load level tested (100 MPa) whereas the failures at lower amplitudes occur (much) earlier. An environmental influence can be assumed as Awatani et al. cooled their specimens with water. If the environment enhances the fatigue process, it is expected that this influence becomes more pronounced the lower the load amplitude is as testing time is increased.

Chapter 5

Outlook and Conclusion

5.1 Outlook

In the present tests the main focus concerning test setup and test control was laid on comparability with former studies (namely [18–22, 37, 38]. To get a deeper insight on the frequency influence, it is crucial to further exclude influences of test control and test setup.

The test control (namely total strain control) of the ultrasonic fatigue testing equipment cannot be changed. Therefore, performing test in total strain control also at 20 Hz might be considered although the influence of test control here is regarded rather small [43].

Concerning the training procedure, it has to be noted that some kind of starting procedure is always needed when using ultrasonic fatigue testing equipment is used. It is not possible to directly start a measurement at high amplitudes as the system has to reach resonance vibration. But the training procedure can be shortened by changing step height and step length. Stanzl-Tschegg and Schönbauer [18] already investigated the influence of the training procedure's step-height comparing 5 MPa steps to 1 MPa steps. No influence on the SN-test's results was found, but the plastic strain amplitudes while training where significantly higher when 5 MPa steps were used. A reduction of the step length of the 20 kHz tests (currently $2 \cdot 10^4$ cycles) may be considered as Stanzl-Tschegg and Schönbauer found that the plastic strain amplitude did not change over the step length. To conform the training procedure, also the step length in the 20 Hz test can be increased. Anyway no saturation is reached within the current step length (of 300 cycles) while training (see Chapter 3.2.1). It has to be considered though that if a frequency effect shifts 20 Hz failures to lower number of cycles, the training procedure should still be short enough so it does not consume most of a specimen's lifetime.

Additionally a more detailed investigation of the fatigue features appearing might be interesting:

Stanzl-Tschegg and Schönbauer [20] found a higher PSB threshold at ultrasonic frequencies compared to conventional frequencies. They suppose that the higher strain rate at ultrasonic testing frequencies leading to a more pronounced hardening of the matrix (together with a superimposed effect of the training procedure) is responsible for this effect. Weidner et al. [21] suppose that PSBs formed at ultrasonic testing frequencies harden very slowly. Therefore an investigation comparing the hardness of PSBs (and surrounding matrix) of specimens tested at different testing frequencies may be interesting. Such an investigation could be performed using SEM with in-situ nanoindentation.

Slip marking evolution could be studied in more detail not only using light optical microscopy but also replica technique. This way it would be possible to investigate also the formation of intrusions at the different testing frequencies in more detail. By using SEM with electron backscatter diffraction (EBSD) the evolution of slip markings could be related to the individual grain's orientation.

Many studies on the dislocation structure of copper at conventional testing frequencies exist [e.g. 28–31] but material and test-setup as well as test control differ widely. Also some TEM investigations of copper tested at ultrasonic frequencies exist [9, 20, 21]. Nevertheless an investigation using specimens tested under the same conditions but different testing frequencies may give more insight on a possible frequency influence. Besides TEM studies also SEM investigations using the back-scattered-electron (BSE) detector (similar to [21]) could be performed to investigate the dislocation structure in more detail. Details on the investigation of dislocation structures using BSE detector are given in [46].

5.2 Conclusion

SN-tests at 20 Hz and 20 kHz have been performed in load control and total strain control respectively. The plastic strain amplitudes were measured and possible influences on the test results have been discussed.

- A clear difference in SN-test results was found if tested at 20 Hz or 20 kHz. Failures did occur earlier at all nominal stress amplitudes if tests were performed at 20 Hz. Besides minor influences of test control and test setup, a frequency effect is held responsible for this behaviour.
- The frequency effect is supposed to manifest mainly in terms of different plastic strain amplitudes. The plastic strain amplitudes were larger when tested at 20 Hz then if tested at 20 kHz. This finding is in good agreement with findings reported in literature.

References

[1] H.-J. Christ, Wechselverformung von Metallen - zyklisches Spannungs-Dehnungs-Verhalten und Mikrostruktur, Werkstoff-Forschung und -Technik ; 9, Springer, Berlin u.a., 1991.

[2] H. A. Mang, G. Hofstetter, Festigkeitslehre, Springer-Lehrbuch : Technik, Springer, Wien u.a., 2000.

[3] W. Schütz, A history of fatigue, Engineering Fracture Mechanics 54 (2) (1996) 263–300.

[4] P. P. Milella, Fatigue and Corrosion in Metals, Springer Milan, Milano, 2013.

[5] J. Schijve, Fatigue of structures and materials, Springer, Dordrecht, 2. edn., 2009.

[6] P. Lukáš, L. Kunz, Specific features of high-cycle and ultra-high-cycle fatigue, Fatigue & Fracture of Engineering Materials & Structures 25 (2002) 747–753.

[7] P. Lukáš, M. Klesnil, Hysteresis Loops in the Microstrain Region, physica status solidi (b) 11 (1) (1965) 127–137.

[8] W. D. J. Callister, D. G. Rethwisch, Materials science and engineering, Wiley, Hoboken, N.J. u.a., 8. , si internat. student edn., 2011.

[9] J. Awatani, K. Katagiri, A. Omura, T. Shiraishi, A study of the fatigue limit of copper, Metallurgical Transactions A 6 (5) (1975) 1029–1034.

[10] S. Suresh, Fatigue of materials, Cambridge Univ. Pr., Cambridge u.a., 2. edn., 1998.

[11] S. Stanzl-Tschegg, Very high cycle fatigue measuring techniques, International Journal of Fatigue 60 (2014) 2–17.

[12] P. Lukáš, M. Klesnil, J. Polák, High cycle fatigue life of metals, Materials Science and Engineering 15 (2–3) (1974) 239–245.

[13] H. Mughrabi, On the life-controlling microstructural fatigue mechanisms in ductile metals and alloys in the gigacycle regime, Fatigue & Fracture of Engineering Materials & Structures 22 (7) (1999) 633–641.

[14] O. B. Pedersen, Cyclic plasticity of metals, Risø National Laboratory, Roskilde, 1991.

[15] N. Thompson, N. Wadsworth, N. Louat, The origin of fatigue fracture in copper, Philosophical Magazine 1 (2) (1956) 113–126.

[16] H. Mughrabi, R. Wang, Cyclic deformation of face-centred cubic polycrystals: a comparison with observations on single crystals, in: N. Hansen, A. Horeswell, T. Leffers, H. Lilholt (Eds.), 2nd Risø International Symposium on Metallurgy and Materials Science, Risø National Laboritory, Roskilde, Denmark, 87–98, 1981.

[17] C. Laird, The fatigue limits of metals, Materials Science and Engineering 22 (1976) 231–236.

[18] S. Stanzl-Tschegg, B. Schönbauer, PSB threshold and fatigue limit of polycrystalline copper in the VHCF-regime, in: J. E. Allison, W. J. Jones, J. M. Laresen, R. O. Ritchie (Eds.), Fourth International Conference on Very High Cycle Fatigue (VHCF-4), TMS (The Minerals & Metals Society), 15–22, 2007.

[19] S. Stanzl-Tschegg, H. Mughrabi, B. Schoenbauer, Life time and cyclic slip of copper in the VHCF regime, International Journal of Fatigue 29 (9-11) (2007) 2050–2059.

[20] S. E. Stanzl-Tschegg, B. Schönbauer, Mechanisms of strain localization, crack initiation and fracture of polycrystalline copper in the VHCF regime, International Journal of Fatigue 32 (6) (2010) 886–893.

[21] A. Weidner, D. Amberger, F. Pyczak, B. Schönbauer, S. Stanzl-Tschegg, H. Mughrabi, Fatigue damage in copper polycrystals subjected to ultrahigh-cycle fatigue below the PSB threshold, International Journal of Fatigue 32 (6) (2010) 872–878.

[22] S. Stanzl-Tschegg, K. Eichinger, A. Weidner, E. Tschegg, J. Bernardi, B. Schönbauer, Role of Impurities and PSBs on Microcracking of Polycrystalline Copper at Very High Numbers of Cycles, Key Engineering Materials 465 (2011) 29–34.

[23] J. C. Figueroa, C. Laird, Crack initiation mechanisms in copper polycrystals cycled under constant strain amplitudes and in step tests, Materials Science and Engineering 60 (1) (1983) 45–58.

[24] N. L. Phung, V. Favier, N. Ranc, F. Valès, H. Mughrabi, Very high cycle fatigue of copper: Evolution, morphology and locations of surface slip markings, International Journal of Fatigue 63 (2014) 68–77.

[25] L. Llanes, C. Laird, Effect of loading mode on the cyclic response and the associated substructure of polycrystalline copper in the high-cycle regime, Fatigue & Fracture of Engineering Materials & Structures 16 (2) (1993) 165–179.

[26] F. L. Liang, C. Laird, Control of intergranular fatigue cracking by slip homogeneity in copper II: Effect of loading mode, Materials Science and Engineering: A 117 (1989) 103–113.

[27] K. Obrtlík, J. Man, J. Polák, Orientation dependence of surface relief topography in fatigued copper single crystals, Materials Science and Engineering: A 234–236 (1997) 727–730.

[28] P. Lukáš, M. Klesnil, J. Krejčí, Dislocations and Persistent Slip Bands in Copper Single Crystals Fatigued at Low Stress Amplitude, physica status solidi (b) 27 (2) (1968) 545–558.

[29] P. Lukáš, M. Klesnil, J. Krejčí, P. Ryš, Substructure of Persistent Slip Bands in Cyclically Deformed Copper, physica status solidi (b) 15 (1) (1966) 71–82.

[30] J. C. Figueroa, S. P. Bhat, R. Delaveaux, S. Murzenski, C. Laird, The Cyclic Stress-Strain Response of Copper at Low Strains .1. Constant Amplitude Testing, Acta Metallurgica 29 (10) (1981) 1667–1678, mj484 Times Cited:120 Cited References Count:28.

[31] B. Yan, A. Hunsche, P. Neumann, C. Laird, Loop patch behavior as affected by incremental loading and cyclic frequency in fatigue, Materials Science and Engineering 79 (1) (1986) 9–14.

[32] P. Lukáš, L. Kunz, L. Navrátilová, O. Bokůvka, Fatigue damage of ultrafine-grain copper in very-high cycle fatigue region, Materials Science and Engineering: A 528 (22–23) (2011) 7036–7040.

[33] M. Papakyriacou, H. Mayer, C. Pypen, H. Plenk Jr, S. Stanzl-Tschegg, Influence of loading frequency on high cycle fatigue properties of b.c.c. and h.c.p. metals, Materials Science and Engineering: A 308 (1–2) (2001) 143–152.

[34] H. Mayer, C. Laird, Influence of cyclic frequency on strain localization and cyclic deformation in fatigue, Materials Science and Engineering: A 187 (1) (1994) 23–35.

[35] N. Marti, N. Saintier, N. Ranc, V. Favier, Frequency effects in high cycle fatigue for polycrystalline pure copper, 2014.

[36] W. P. Mason, W. A. Wood, Fatigue Mechanism in fcc Metals at Ultrasonic Frequencies, Journal of Applied Physics 39 (12) (1968) 5581–5584.

[37] K. Eichinger, Gleiterscheinungen und Rissbildung bei Wechselbeanspruchung von polykristallinem Kupfer, Diplomarbeit, Technische Universität Wien, 2008.

[38] B. Schönbauer, Ermüdungsverhalten von polykristallinem Kupfer bei Wechselbeanspruchung im Ultraschallbereich (20 kHz), Diplomarbeit, Technische Universität Wien, 2008.

[39] S. Stanzl, A new experimental method for measuring life time and crack growth of materials under multi-stage and random loadings, Ultrasonics 19 (6) (1981) 269–272.

[40] H. Mayer, Ultrasonic Fatigue Testing Equipment, Institute of Physics and Material Science, 2009.

[41] M. Papakyriacou, H. Mayer, H. Plenk Jr, S. Stanzl-Tschegg, Cyclic plastic deformation of tantalum and niobium at very high numbers of cycles, Materials Science and Engineering: A 325 (1–2) (2002) 520–524.

[42] Deutsches Kupferinstitut Berufsverband e.V., Werkstoffdatenblatt Cu-ETP, URL http://www.kupferinstitut.de/front_frame/pdf/Cu-ETP.pdf, 2014.

[43] J. Polák, M. Klesnil, P. Lukáš, High cycle plastic stress-strain response of metals, Materials Science and Engineering 15 (2–3) (1974) 231–237.

[44] B. Schönbauer, Personal communication, 2008.

[45] W. Hessler, H. Müllner, B. Weiss, "Ermüdungsgrenze" in vielkristallinem Kupfer nach hochfrequenter Wechselverformung (20kHz), in: Frühjahrstagung, vol. 15 of *Verhandlungen*, Deutsche Physikalische Gesellschaft, 340, 1980.

[46] A. Weidner, C. Blochwitz, W. Skrotzki, W. Tirschler, Formation of slip steps and growth of extrusions within persistent slip bands in cyclically deformed polycrystals, Materials Science and Engineering: A 479 (1–2) (2008) 181–190.

Appendix A

Certificate Cu-ETP

ALLMESON

Universität f. Bodenkultur
Inst. f. Physik u. Materialwissenschaft
Andrea Perlega
Peter Jordan Str. 82
1190 Wien
Österreich

Abnahmeprüfzeugnis EN 10204/3.1
(Abschrift)

Datum:	28.05.13
Seite:	1
Ihre Bestellnr.:	Frau Perlega
Unsere Lieferungsnr.:	VLA1300838 vom 24.05.13
Ansprechpartner/in:	Stefan Zwieg
E-Mail:	szwieg@allmeson.de
Tel.:	06104-4059-81 (Fax: -90)

Artikel	Menge	ME	Charge
Kupfer Rundstangen Cu-ETP (CW004A) DIN: E-Cu58/57 (2.0065/60) **Ø 15 mm** 5 St. a 2 mtr.	**16,00**	**KG**	**AM1301846**

Chemische Zusammensetzung:

Cu	99,990 %

Mechanische Werte:

Zugfestigkeit Rm:	271,000 N/qmm
Zugfestigkeit Rm min.:	250,000 N/qmm
Zugfestigkeit Rm max.:	300,000 N/qmm
Dehngrenze Rp 0,2:	203,000 N/qmm
Härte (HB):	87,000
Härte (HB) min.:	70,000
Härte (HB) max.:	95,000
Bruchdehnung (A5):	12,000 %

Es wird bestätigt, dass die Lieferung den Vereinbarungen bei der Bestellung entspricht.

Mit freundlichen Grüßen
ALLMESON GMBH

Appendix B

Average Grain Intersect Method

Using an optical microscope (Leica DM 4000 M) images of the surface of specimen U1 were taken. This specimen did not show a smooth specimen surface but grain boundaries after electrolytic polishing due to some mistake in the polishing process. Three images with different polarisation (Figures B.1 to B.3) were taken of each of three different circumferential positions in the gauge length. These images were overlaid digitally later on and the grain boundaries were digitally gone over. The procedure is illustrated for one position by the images shown in Figures B.1 to B.5.

The so produced images (Figures B.5 to B.7) were used to measure the grain size using the grain intersect method specified in DIN 2624. Seven lines were laid over the image and intersections with grain boundaries were counted manually. The grain sizes obtained are listed in Table B.1 giving a mean grain size of 39 µm.

TABLE B.1: Grain sizes

Image No.	Figure	Grain Size
01	Figure B.5	38 µm
02	Figure B.6	38 µm
03	Figure B.7	42 µm

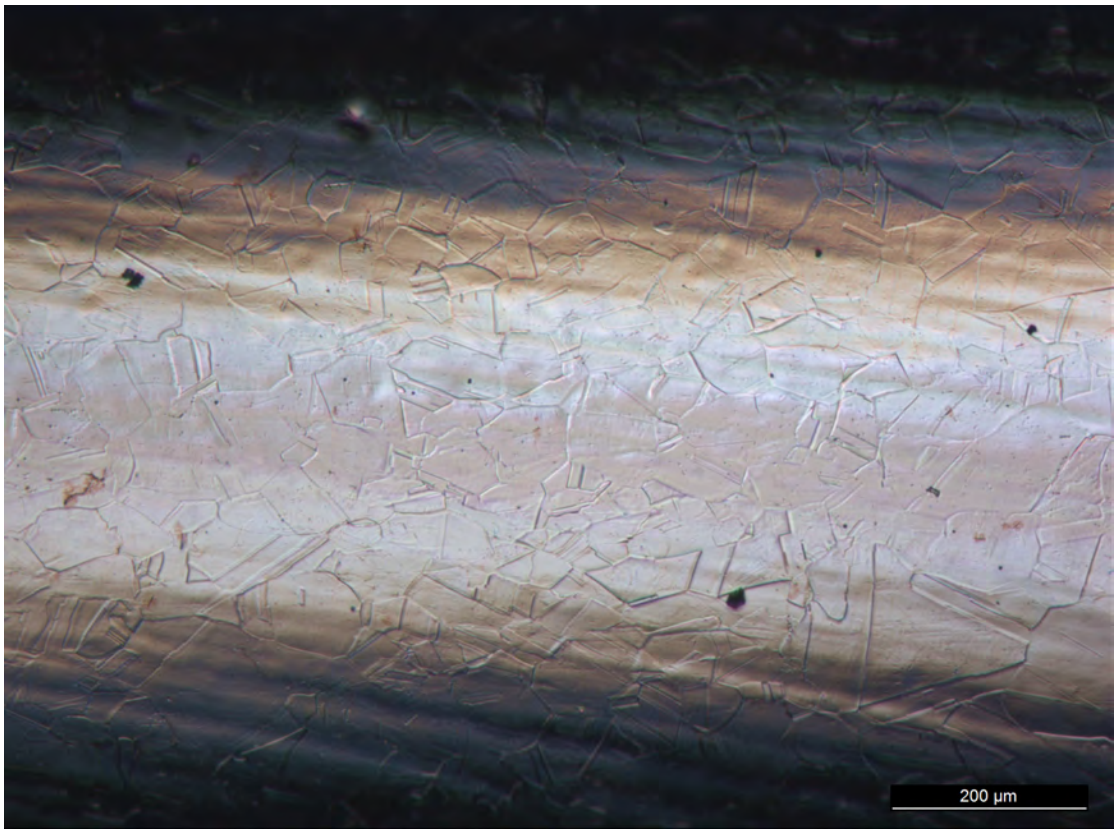

FIGURE B.1: Specimen surface U1.

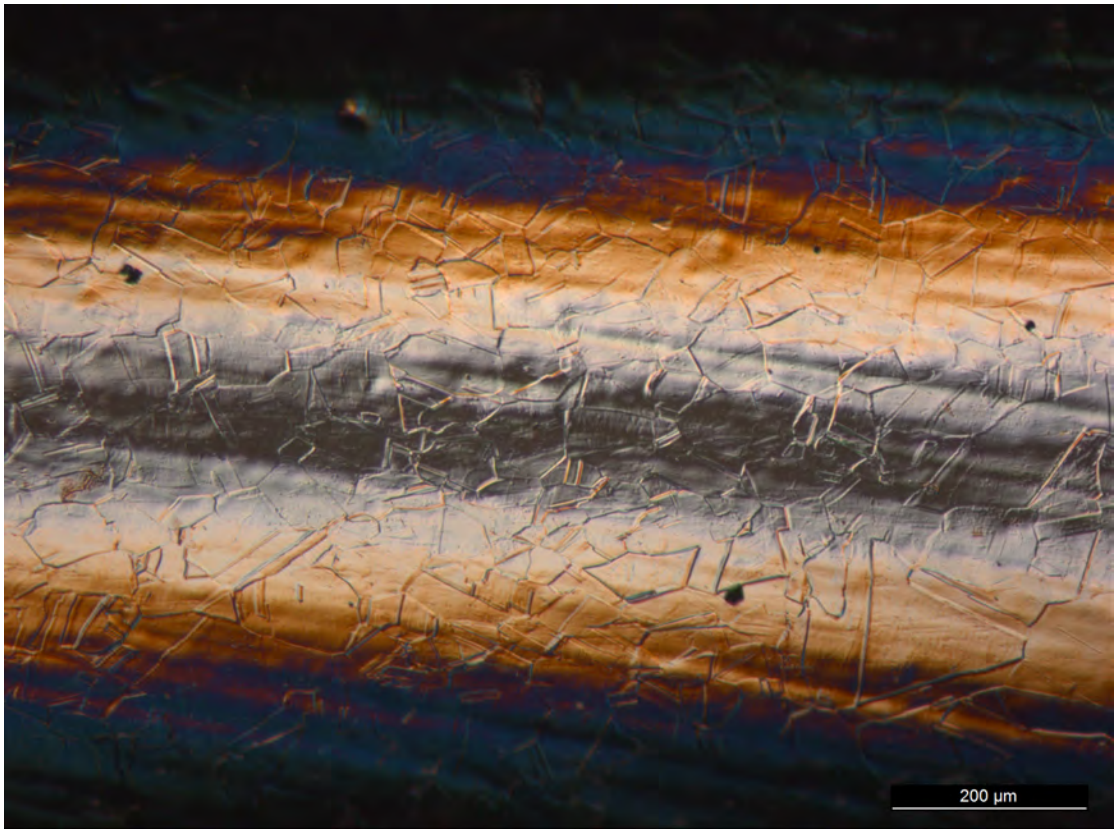

FIGURE B.2: Specimen surface U1.

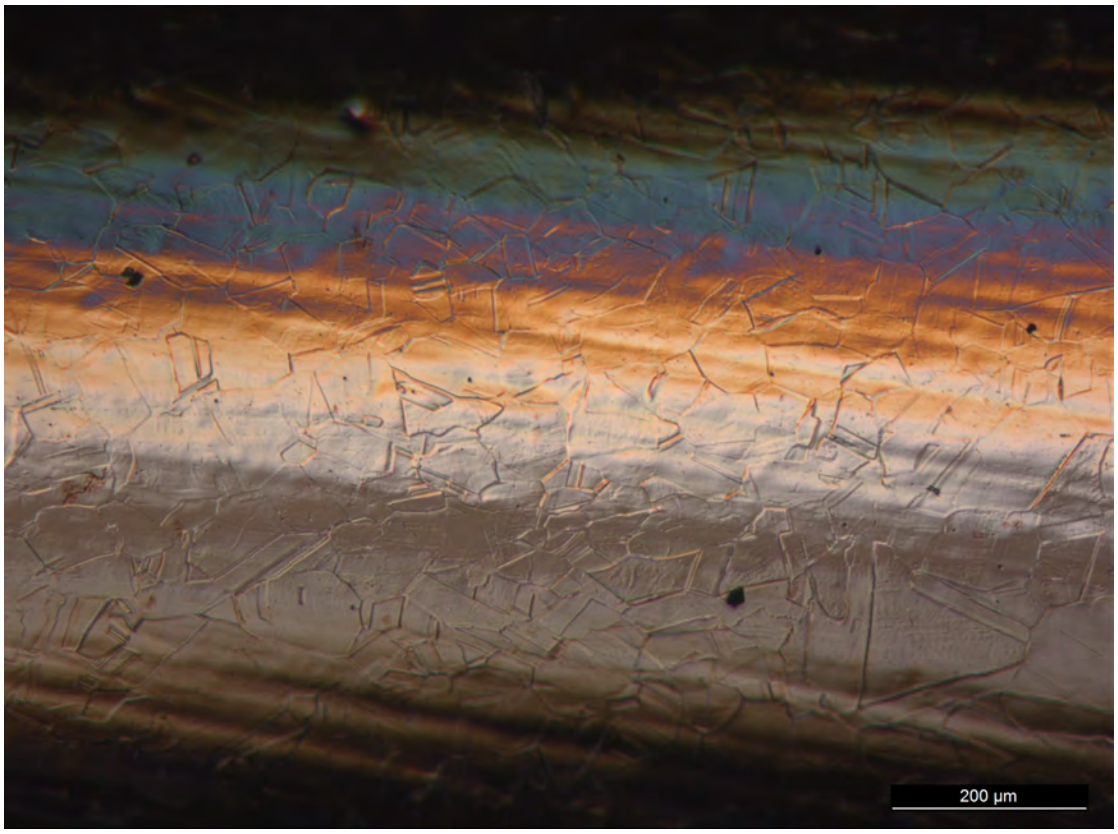

FIGURE B.3: Specimen surface U1.

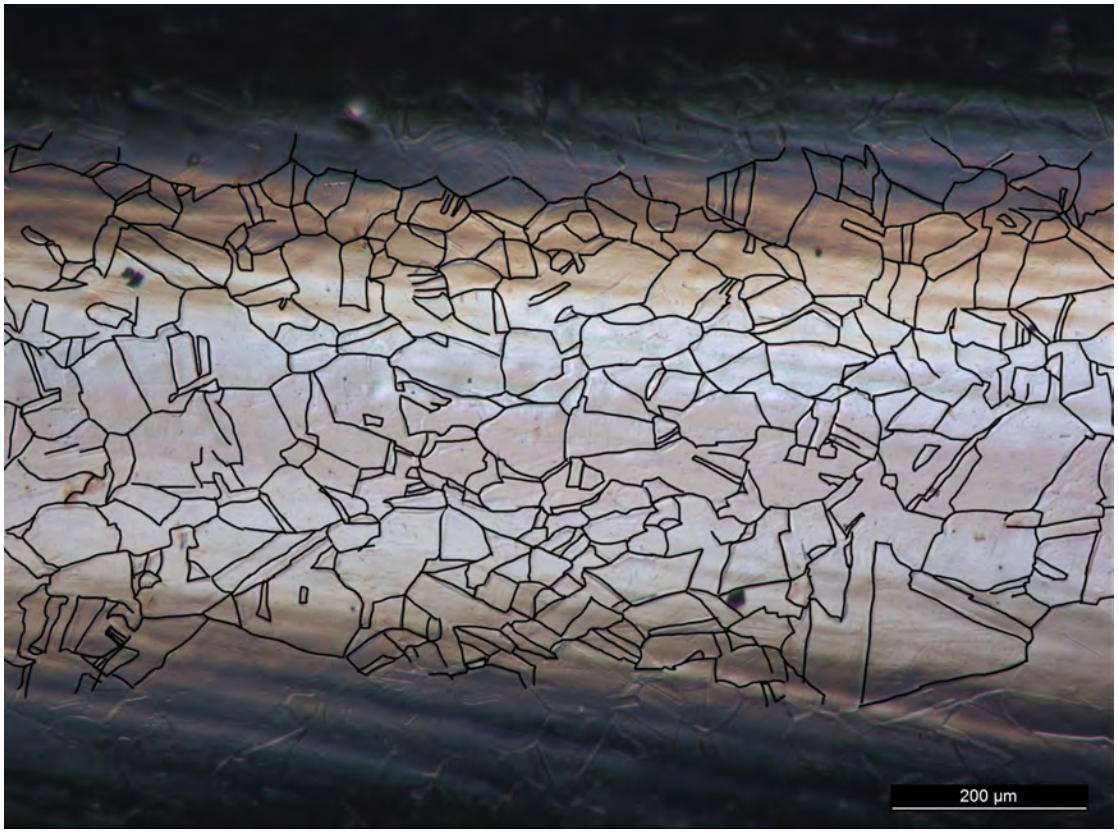

FIGURE B.4: Grainboundaries.

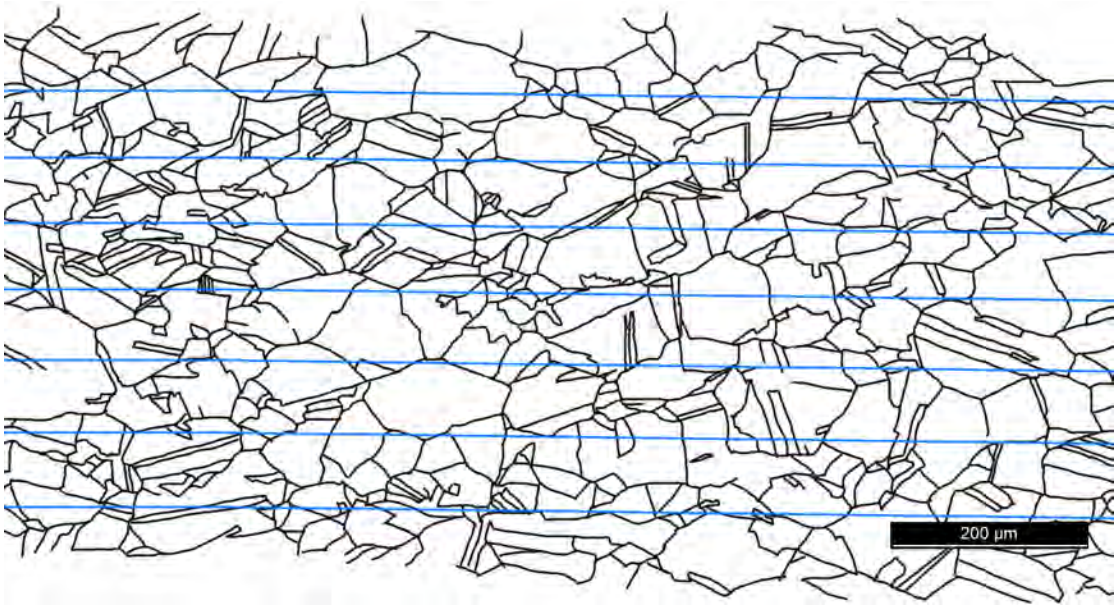

FIGURE B.5: Grain intersect method (Image No. 01).

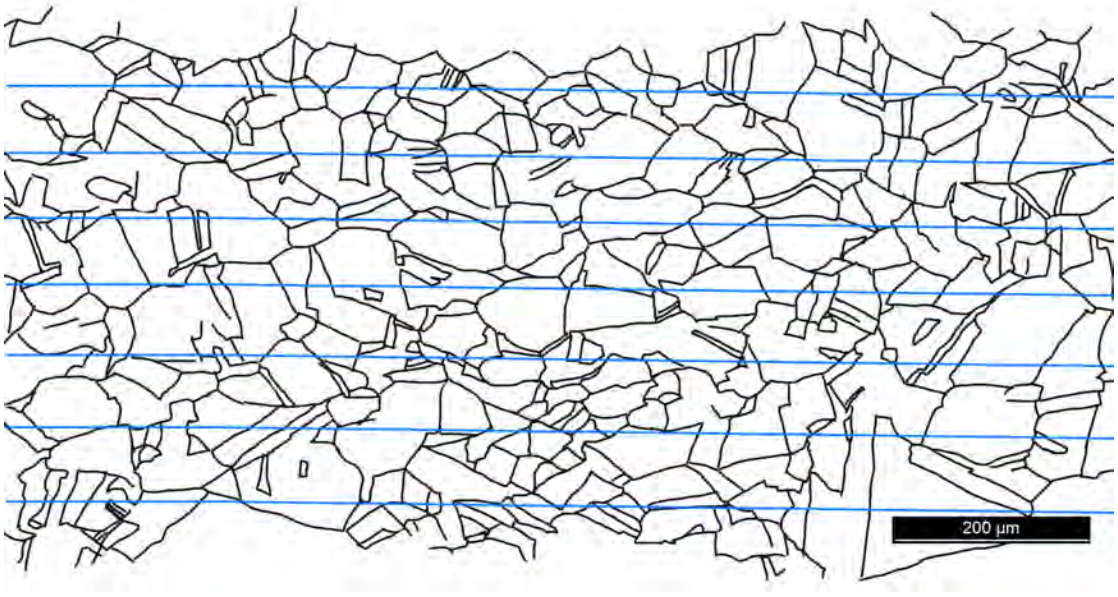

FIGURE B.6: Grain intersect method (Image No. 02).

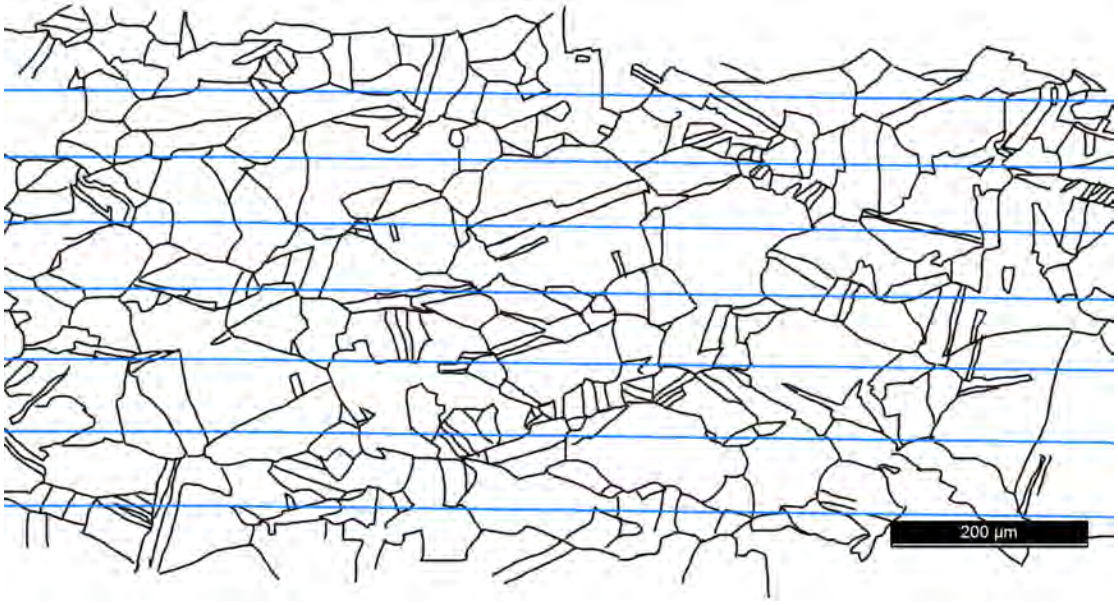

FIGURE B.7: Grain intersect method (Image No. 03).

Appendix C

Specifications EDC 580

C.1 PID Parameters

The PID parameters used for testing at 20 Hz with hourglass shaped specimens (specimen shape given in Chapter 2.2, Figure 2.2) are listed in Table C.1.

Table C.1: PID Parameters

Parameter	Value
PosP	500
SpeedP	2354
SpeedI	28
Speed FFP	116

C.2 Sensor EEPROM

An analouge Sensor (Part identification number 580) is connected via the port X25B to the EDC 580 controller. The following sensor data (listed in Table C.2) is written to the EEPROM.

Table C.2: Sensor EEPREOM

Sensor type	Strain gauge
Nominal value	1
Sensitivity at nominal value	0.525 mV/V
Range limit min. & max.	150 %
Sensor offset	0
Maximum exitation voltage	5 V
Impedance	120 Ω

Appendix D

Data Evaluation

The data obtained in the plastic strain amplitude measurements is evaluated using python programs. These are listed in the following.

D.1 Data Recorded while Training Procedure

```
import numpy as np

e_1 = []
e_2 = []
e_3 = []
e_pl = []
e_tot = []
niveau = []
cycle = []
e_pl_l =[]
e_tot_l=[]

####first file

##import data to array
Zeit,Weg,Kraft,Zyklen,Sen4,DMS=np.loadtxt("hysterese_DMS_3.txt",skiprows=4,
    unpack=True)

## convert np.array in list
Zyklen_liste=Zyklen.tolist()
Kraft_liste=Kraft.tolist()

#possible number of cycles to start with
a=[29., 30., 31., 32., 33., 34., 35., 36., 37., 38.]
```

```
Z_diff=[0.,1196.,1196.,1194.,1200.,893.,893.,903.,895.,900.,895.,895.,895.]

for l in range (0,13):
    for k in range (0,10):
        a[k]=a[k]+Z_diff[l]

    for j in range (0,15):
## define start for number of cycles
        for k in range (0,10):
            if a[k] in Zyklen_liste:
                n_start=Zyklen_liste.index(a[k])

        for k in range (0,10):
            a[k]=a[k]+99
            if a[k] in Zyklen_liste:
                n_index= Zyklen_liste.index(a[k])
        n1=n_start

        for i in range (0,7):
            Z=Zyklen[n_start]+10.*float(i)
##nZ ... entries for this cycle -1
            nZ=Zyklen_liste.count(Z)-1

##calculation e_pl
            n2=n1+int(nZ/2)
            n3=n2+1
            n4=n1+nZ

            if Kraft[n3] > 0:
                n2=n2+1
                n3=n2+1

            if Kraft[n2] < 0:
                n2=n2-1
                n3=n2+1

##strain at beginning of cycle
            e_1.append(Sen4[n1]*(-1.))
##strain at end of cycle
            e_3.append(Sen4[n4]*(-1.))
##calculate zero crossing
##f(x) = m*x + b
            x1 = Sen4[n2]*(-1.)
            y1 = Kraft[n2]
            x2 = Sen4[n3]*(-1.)
            y2 = Kraft[n3]

            m=(y1-y2)/(x1-x2)
```

```
            b=y1-m*x1
            e_2.append((-1.)*b/m)

            e_pl.append(0.0005*abs(e_1[-1]-e_2[-1]))
            niveau.append(10+l*5)
            cycle.append(Zyklen[n1])

##calculate e_tot
            for o in range (n1,n1+nZ):
                if Kraft[o+1] < Kraft[o]:
                    K_min=Kraft[o+1]
            for o in range (n1,n1+int(nZ/2)):
                if Kraft[o+1] > Kraft[o]:
                    K_max=Kraft[o+1]

            n_o1=Kraft_liste.index(K_max)
            n_o2=Kraft_liste.index(K_min)

            e_tot.append(0.0005*abs(Sen4[n_o1]-Sen4[n_o2]))

            n1=n4+1

    e_pl_l.append(e_pl[-1])
    e_tot_l.append(e_tot[-1])

Z_letzt = cycle[-1]


####second file
Zeit2,Weg2,Kraft2,Zyklen2,Sen42,DMS2=np.loadtxt("hysterese_DMS_4.txt",
    skiprows=4,unpack=True)

Zyklen_liste2=Zyklen2.tolist()
Kraft_liste2=Kraft2.tolist()

a=[29., 30., 31., 32., 33., 34., 35., 36., 37., 38.]
Z_diff=[0.,1196.,1196.,1194.,1200.,1192.,1191.,1202.,1194.,1199.]

for l in range (0,10):
    for k in range (0,10):
        a[k]=a[k]+Z_diff[l]

    for j in range (0,15):

        for k in range (0,10):
            if a[k] in Zyklen_liste2:
                n_start=Zyklen_liste2.index(a[k])
```

```
for k in range (0,10):
    a[k]=a[k]+99
    if a[k] in Zyklen_liste2:
        n_index= Zyklen_liste2.index(a[k])
n1=n_start

for i in range (0,7):
    Z=Zyklen2[n_start]+10.*float(i)

    nZ=Zyklen_liste2.count(Z)-1
    n2=n1+int(nZ/2)
    n3=n2+1
    n4=n1+nZ

    if Kraft[n3] > 0:
        n2=n2+1
        n3=n2+1
    if Kraft[n2] < 0:
        n2=n2-1
        n3=n2+1

    e_1.append(Sen42[n1]*(-1.))
    e_3.append(Sen42[n4]*(-1.))

    x1 = Sen42[n2]*(-1.)
    y1 = Kraft2[n2]
    x2 = Sen42[n3]*(-1.)
    y2 = Kraft2[n3]
    m=(y1-y2)/(x1-x2)
    b=y1-m*x1
    e_2.append((-1.)*b/m)

    e_pl.append(0.0005*abs(e_1[-1]-e_2[-1]))
    niveau.append(75+l*5)
    cycle.append(Z_letzt+Zyklen2[n1])

    for o in range (n1,n1+nZ):
        if Kraft2[o+1] < Kraft2[o]:
            K_min=Kraft2[o+1]
    for o in range (n1,n1+int(nZ/2)):
        if Kraft2[o+1] > Kraft2[o]:
            K_max=Kraft2[o+1]

    n_o1=Kraft_liste2.index(K_max)
    n_o2=Kraft_liste2.index(K_min)

    e_tot.append(0.0005*abs(Sen42[n_o1]-Sen42[n_o2]))
    n1=n4+1
```

```
        e_pl_l.append(e_pl[-1])
        e_tot_l.append(e_tot[-1])

##output
f_ausgabe=open('e_pl.txt',mode='w')

for i, item in enumerate(e_pl):
        f_ausgabe.write(str(i)+'\t'+str(niveau[i])+ "\t" +str(cycle[i])+ "\t" +
        str(e_tot[i])+ "\t"+ str(e_pl[i])+'\n')

f_ausgabe.close()

f_ausgabe=open('e_pl_l.txt',mode='w')

for i, item in enumerate(e_pl_l):
        f_ausgabe.write(str(10+i*5)+ "\t" + str(e_tot_l[i])+ "\t" + str(e_pl_l[
        i])+'\n')

f_ausgabe.close()
```

D.2 Data Recorded while SN-testing at 100 MPa

```
import numpy as np

e_1 = []
e_2 = []
e_3 = []
e_pl = []
e_tot = []
niveau = []
cycle = []
N_cycle = []
force = []

##import data to array
Zeit,Weg,Kraft,Zyklen,Sen4,DMS=np.loadtxt("hysterese_N34.txt",skiprows=4,
    unpack=True)

##convert np.array in list
Zyklen_liste=Zyklen.tolist()
Kraft_liste=Kraft.tolist()

##Number of cycles at which 100 MPa niveau starts
Z_start=26941.
n_start=Zyklen_liste.index(Z_start)
```

```
n1=n_start

for i in range (0,39):
    Z=Zyklen[n1]
##nZ ... entries for this cycle -1
    nZ=Zyklen_liste.count(Z)-1

##calculation e_pl
    n2=n1+int(nZ/2)
    n3=n2+1
    n4=n1+nZ

    if Kraft[n3] > 0:
        n2=n2+1
        n3=n2+1
    if Kraft[n2] < 0:
        n2=n2-1
        n3=n2+1

##strain at beginning of cycle
    e_1.append(Sen4[n1])
##strain at end of cycle
    e_3.append(Sen4[n4])
##calculate zero crossing
##f(x) = m*x + b
    x1 = Sen4[n2]
    y1 = Kraft[n2]
    x2 = Sen4[n3]
    y2 = Kraft[n3]

    m=(y1-y2)/(x1-x2)
    b=y1-m*x1
    e_2.append((-1.)*b/m)

    e_pl.append(0.0005*abs(e_1[-1]-e_2[-1]))
    niveau.append(100)
    cycle.append(Zyklen[n1])
    N_cycle.append(Zyklen[n1]-Z_start+21)

##calculate e_tot
    for o in range (n1,n1+nZ):
        if Kraft[o+1] < Kraft[o]:
            K_min=Kraft[o+1]
    for o in range (n1,n1+int(nZ/2)):
        if Kraft[o+1] > Kraft[o]:
            K_max=Kraft[o+1]

        n_o1=Kraft_liste.index(K_max)
```

```
            n_o2=Kraft_liste.index(K_min)

        force.append(K_max/(1.5*1.5*3.14))
        e_tot.append(0.0005*abs(Sen4[n_o1]-Sen4[n_o2]))

        n1=n4+1

##output
f_ausgabe=open('e_pl_N34.txt',mode='w')

for i, item in enumerate(e_pl):
    f_ausgabe.write(str(i)+'\t'+str(niveau[i])+ "\t" +str(cycle[i])+ "\t" +
    str(N_cycle[i])+"\t"+str(force[i])+ "\t" +str(e_tot[i])+ "\t"+ str(e_pl
    [i])+'\n')

f_ausgabe.close()
```

D.3 Data Recorded while SN-testing at 70 MPa

```
import numpy as np

e_1 = []
e_2 = []
e_3 = []
e_pl = []
e_tot = []
niveau = []
cycle = []
N_cycle = []
force = []

##import data to array

Zeit,Weg,Kraft,Zyklen,Sen4,DMS=np.loadtxt("hysterese_N35.txt",skiprows=4,
    unpack=True)

##convert np.array in list
Zyklen_liste=Zyklen.tolist()
Kraft_liste=Kraft.tolist()


##Number of cycles at which 70 MPa niveau starts
Z_start=17971
n_start=Zyklen_liste.index(Z_start)
n1=n_start
```

```
for i in range (0,36527):
##nZ ... entries for this cycle -1
    Z=Zyklen[n1]
    nZ=Zyklen_liste.count(Z)-1

##calculation e_pl
    n2=n1+int(nZ/2)
    n3=n2+1
    n4=n1+nZ

    if Kraft[n3] > 0:
        n2=n2+1
        n3=n2+1

    if Kraft[n2] < 0:
        n2=n2-1
        n3=n2+1

##strain at beginning of cycle
    e_1.append(Sen4[n1])
##strain at end of cycle
    e_3.append(Sen4[n4])
##calculate zero crossing
##f(x) = m*x + b
    x1 = Sen4[n2]
    y1 = Kraft[n2]
    x2 = Sen4[n3]
    y2 = Kraft[n3]

    m=(y1-y2)/(x1-x2)
    b=y1-m*x1
    e_2.append((-1.)*b/m)

    e_pl.append(0.0005*abs(e_1[-1]-e_2[-1]))
    niveau.append(100)
    cycle.append(Zyklen[n1])
    N_cycle.append(Zyklen[n1]-Z_start+21)

##calculate e_tot
    for o in range (n1,n1+nZ):
        if Kraft[o+1] < Kraft[o]:
            K_min=Kraft[o+1]
    for o in range (n1,n1+int(nZ/2)):
        if Kraft[o+1] > Kraft[o]:
            K_max=Kraft[o+1]

        n_o1=Kraft_liste.index(K_max)
        n_o2=Kraft_liste.index(K_min)
```

```
        force.append(K_max/(1.52*1.52*3.14))
        e_tot.append(0.0005*abs(Sen4[n_o1]-Sen4[n_o2]))

        n1=n4+1

##output
f_ausgabe=open('e_pl_N35.txt',mode='w')

for i, item in enumerate(e_pl):
    f_ausgabe.write(str(i)+'\t'+str(niveau[i])+ "\t" +str(cycle[i])+ "\t" +
    str(N_cycle[i])+"\t"+str(force[i])+ "\t" +str(e_tot[i])+ "\t"+ str(e_pl
    [i])+'\n')

f_ausgabe.close()
```

Appendix E

Evolution of slip markings

E.1 20 Hz Test

To investigate the evolution of slip markings, Specimen N25 was used. The specimen's lifetime was estimated (by the tests already performed) $4.5 \cdot 10^5$ cycles. This estimated lifetime was divided by ten to set the number of cycles after which a light optical observation should be performed. To make sure no stresses are applied to the specimen when mounting it into the load frame, additionally an image before and after mounting was taken. Figure E.1 shows the specimen before mounting. Figure E.2 shows the specimen after mounting in the load frame. No slip markings resulting from stresses during mounting are visible. (In preliminary tests with another load frame, it was not possible to mount a specimen without getting slip markings.)

Table E.1 lists the images and the number of cycles when they were taken. The specimen was subjected the same training procedure as all other 20 Hz SN-tests (for details see Chapter 2.5). The counting of number of cycles started after the training procedure was finished (Figure E.3). Slip markings resulting from the training procedure are already visible. Figures E.4 to E.10 show the evolution of slip markings on the specimen surface during fatigue testing. The density of slip markings on the specimen surface increases with number of cycles. A growing crack is already visible after $4.49 \cdot 10^4$ cycles (Figure E.4). The last image was taken after $3.14 \cdot 10^5$ cycles (Figure E.10). The specimen failed after $3.95 \cdot 10^5$ cycles.

FIGURE E.1: Specimen N25 after electrolytic polishing, before testing.

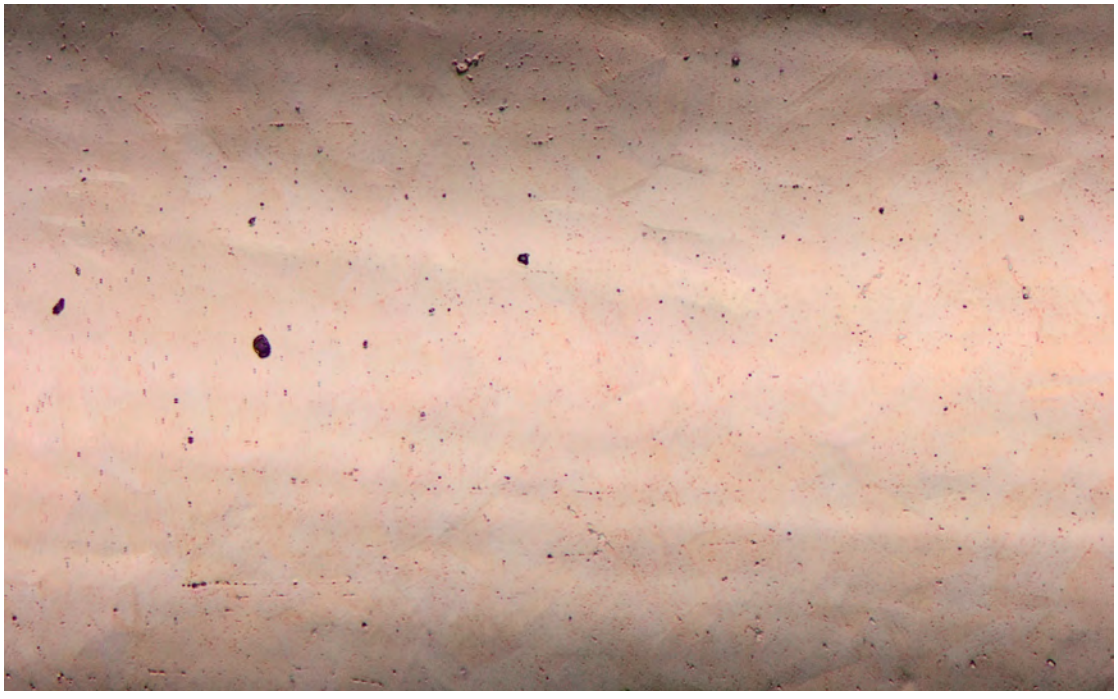

FIGURE E.2: Specimen N25 after mounting into the load frame.

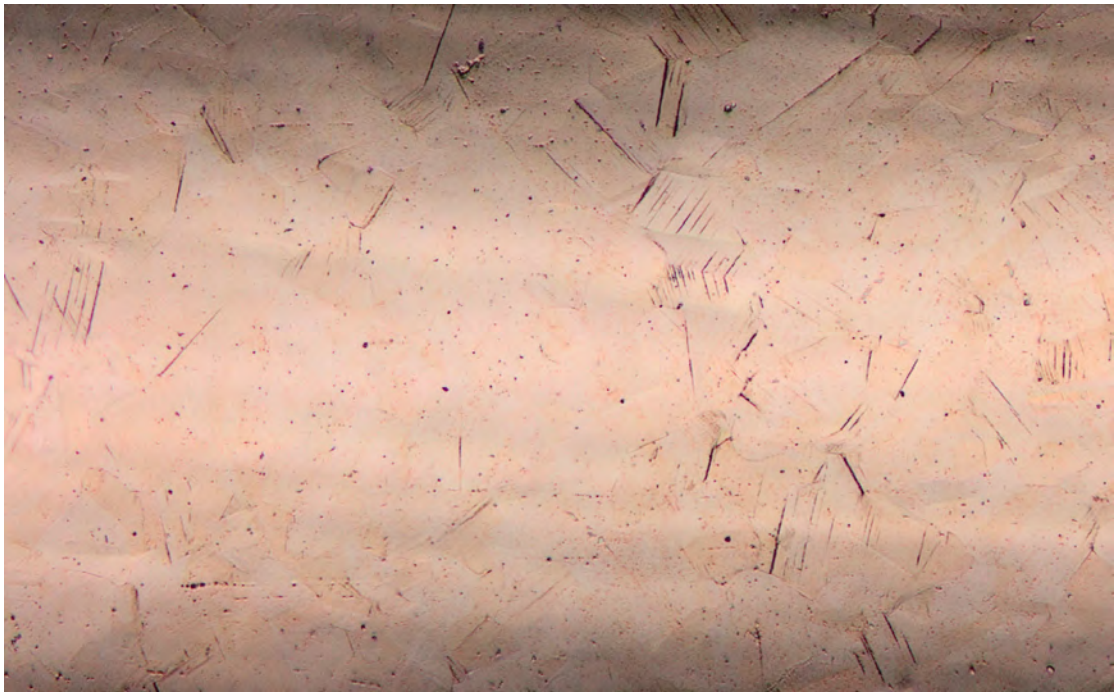

FIGURE E.3: Specimen N25 after training procedure $N = 0$ cycles.

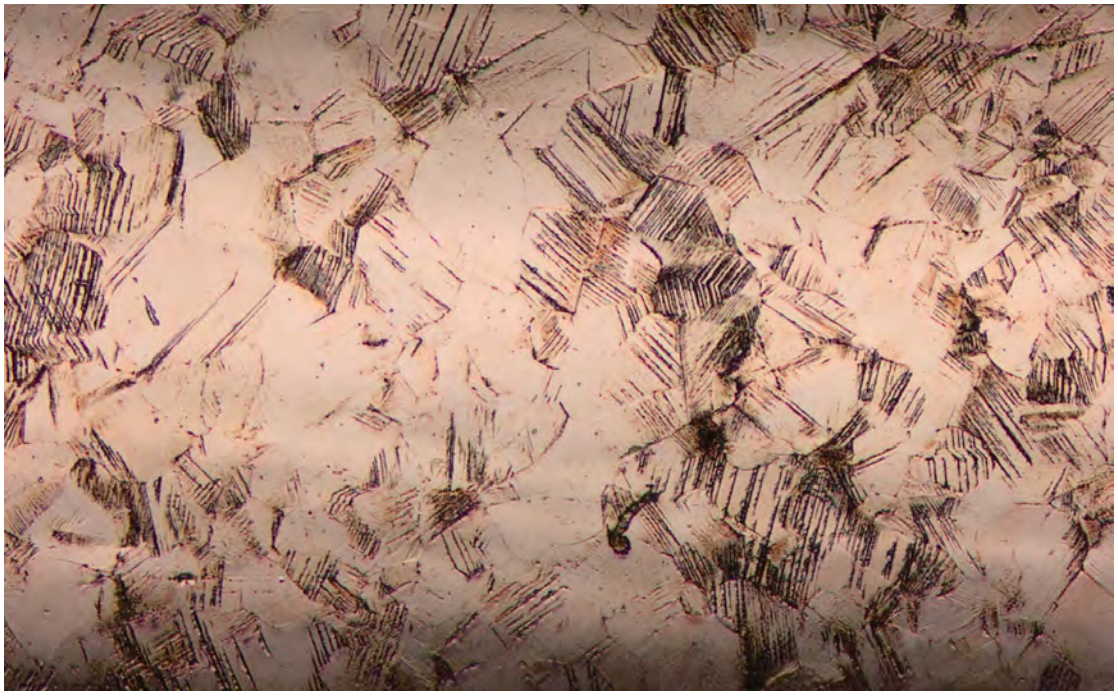

FIGURE E.4: Specimen N25 after $N = 4.49 \cdot 10^4$ cycles.

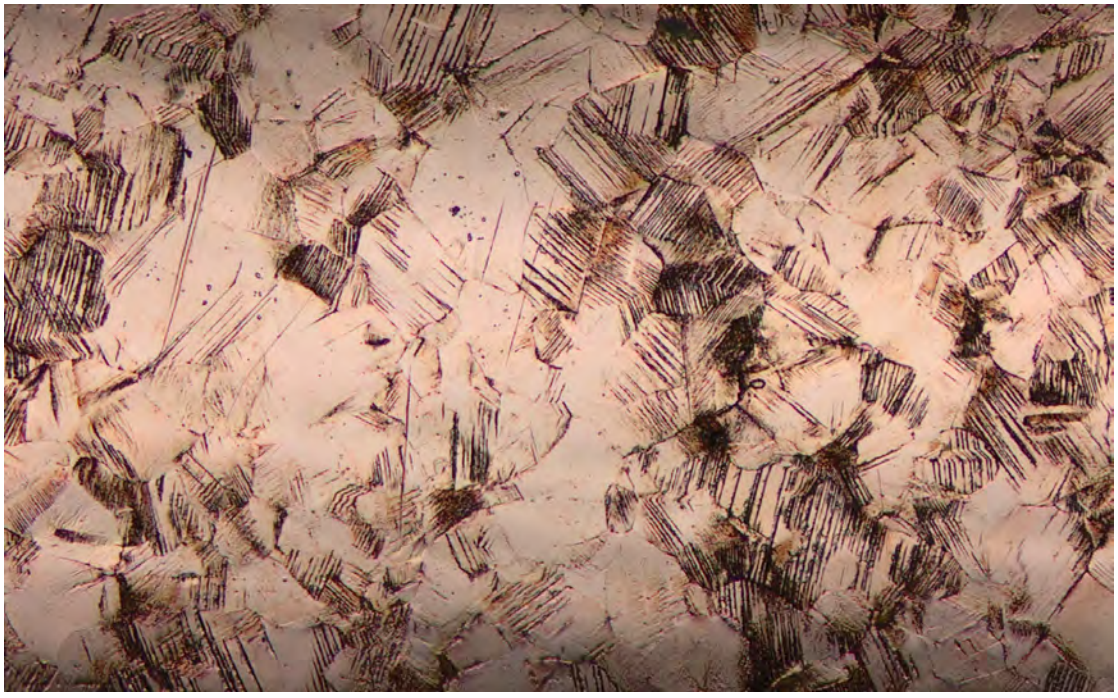

FIGURE E.5: Specimen N25 after $N = 8.98 \cdot 10^4$ cycles.

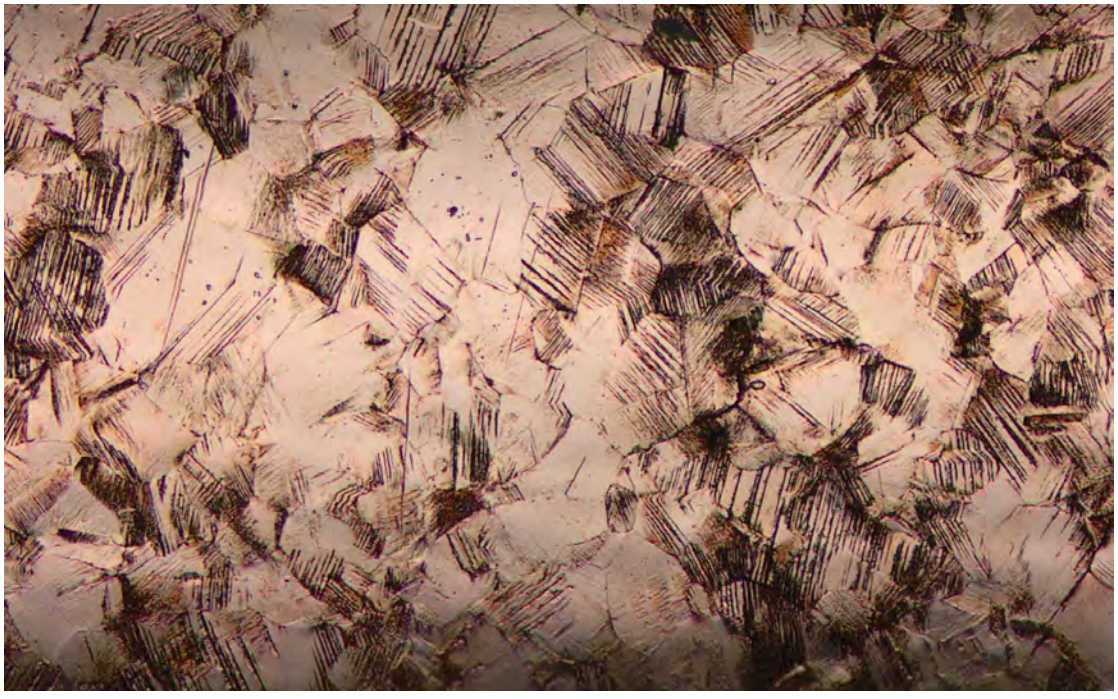

FIGURE E.6: Specimen N25 after $N = 1.35 \cdot 10^5$ cycles.

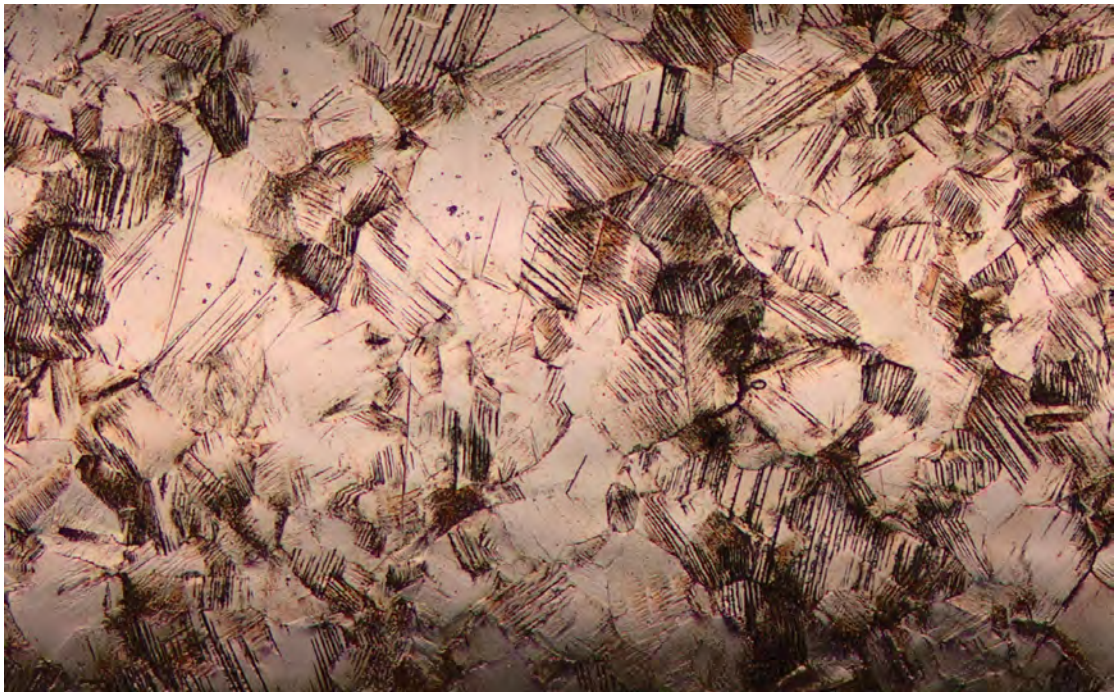

FIGURE E.7: Specimen N25 after $N = 1.80 \cdot 10^5$ cycles.

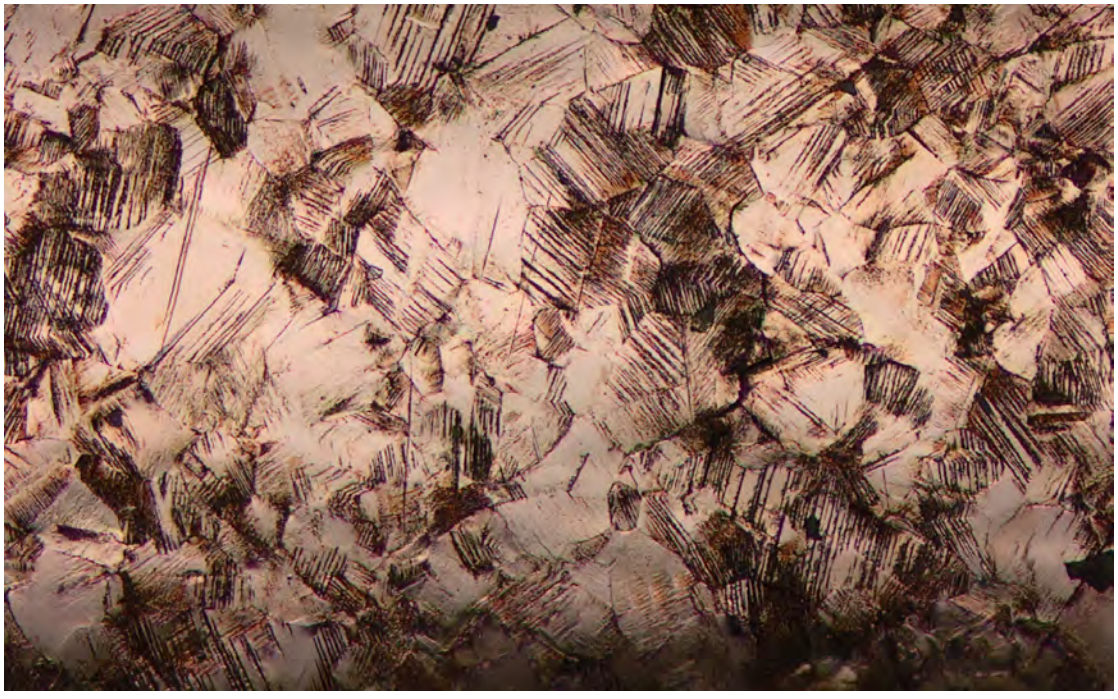

FIGURE E.8: Specimen N25 after $N = 2.25 \cdot 10^5$ cycles.

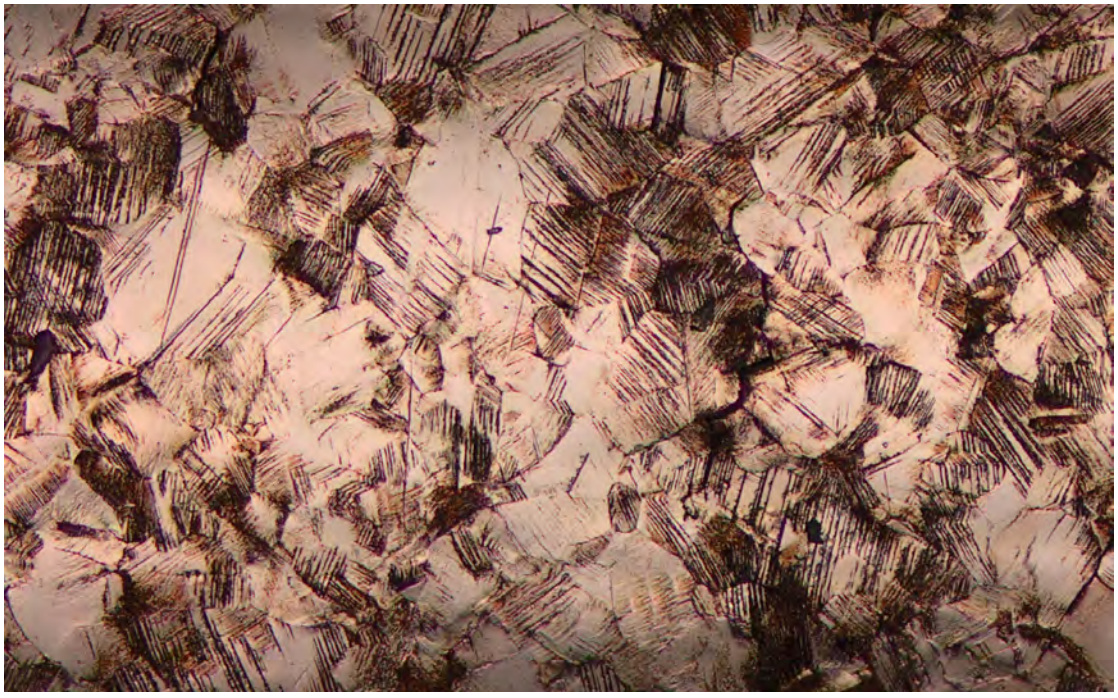

FIGURE E.9: Specimen N25 after $N = 2.70 \cdot 10^5$ cycles.

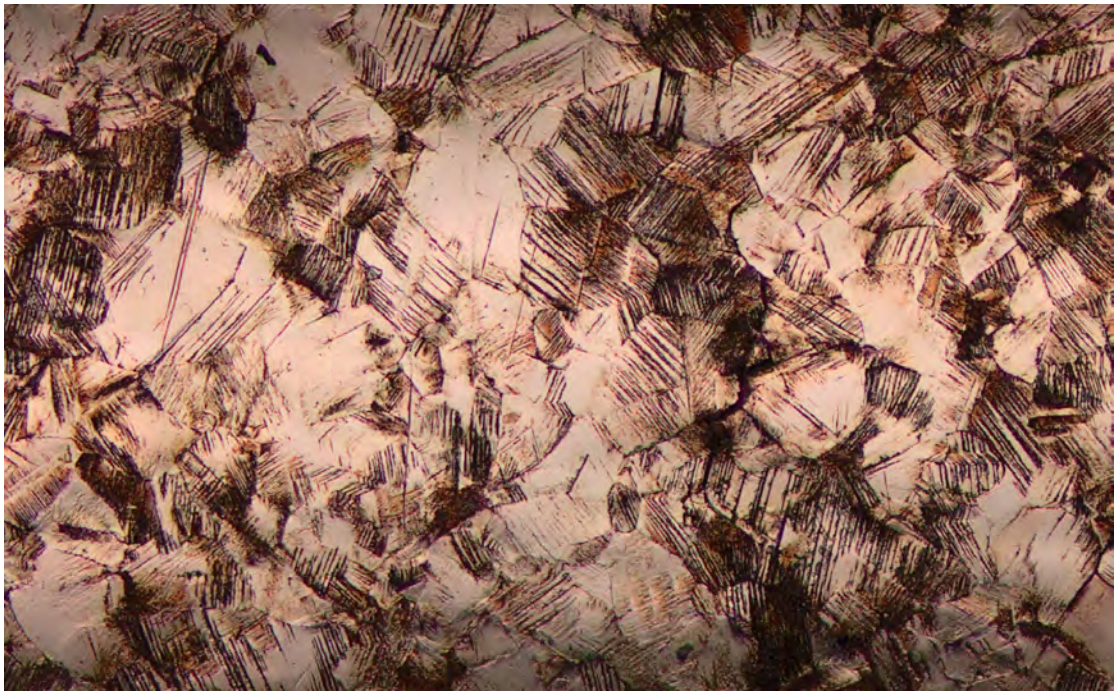

FIGURE E.10: Specimen N25 after $N = 3.14 \cdot 10^5$ cycles.

TABLE E.1: Images taken during 20 Hz SN-test (specimen N25) and corresponding number of cycles

Image No.	Figure	Number of cycles
1	Figure E.1	0
2	Figure E.2	0
3	Figure E.3	0
4	Figure E.4	$4.49 \cdot 10^4$
5	Figure E.5	$8.98 \cdot 10^4$
6	Figure E.6	$1.35 \cdot 10^5$
7	Figure E.7	$1.80 \cdot 10^5$
8	Figure E.8	$2.25 \cdot 10^5$
9	Figure E.9	$2.70 \cdot 10^5$
10	Figure E.10	$3.14 \cdot 10^5$

TABLE E.2: Images taken during 20 kHz SN-test (specimen U21) and corresponding number of cycles

Image No.	Figure	Number of cycles
1	Figure E.11	0
2	Figure E.12	0
3	Figure E.13	$8.10 \cdot 10^5$
4	Figure E.14	$1.62 \cdot 10^6$
5	Figure E.15	$2.43 \cdot 10^6$
6	Figure E.16	$3.24 \cdot 10^6$
7	Figure E.17	$4.05 \cdot 10^6$
8	Figure E.18	$4.86 \cdot 10^6$
9	Figure E.19	$5.67 \cdot 10^6$
10	Figure E.20	$6.48 \cdot 10^6$
11	Figure E.21	$7.29 \cdot 10^6$
12	Figure E.22	$8.10 \cdot 10^6$
13	Figure E.23	$8.91 \cdot 10^6$

FIGURE E.11: Specimen U21 after electrolytic polishing, before testing.

E.2 20 kHz Test

To investigate the evolution of slip markings at 20 kHz, Specimen U21 was used. The specimen's lifetime was estimated by the tests already performed. The estimated lifetime ($8.1 \cdot 10^6$ cycles) was divided by ten to set the number of cycles after which a light optical observation should be performed. Due to the repeated mounting of the specimen, it failed at the thread. Therefore, no fatigue failure was achieved.

Table E.2 lists the images and the number of cycles when they were taken. Figure E.11 shows the specimen surface after electrolytic polishing before any load was applied. The specimen was subjected to the same training procedure as all other SN-tests at 20 kHz (for details see Chapter 2.5). The counting of number of cycles started after the training procedure was finished. Slip markings resulting from the training procedure are already visible (Figure E.12) at this stage. Figures E.13 to E.23 show the evolution of slip markings on the specimen surface during fatigue testing[1].

[1]To restart the test, a starting procedure where the amplitude is increased stepwise has to be performed. Within this starting procedure approximately $5 \cdot 10^4$ cycles were gathered (over a range of smaller amplitudes reaching from approximately 10 to 90 MPa) each time. The cycles gathered during the starting procedure were not counted as number of cycles to failure as the amplitudes were significantly lower.

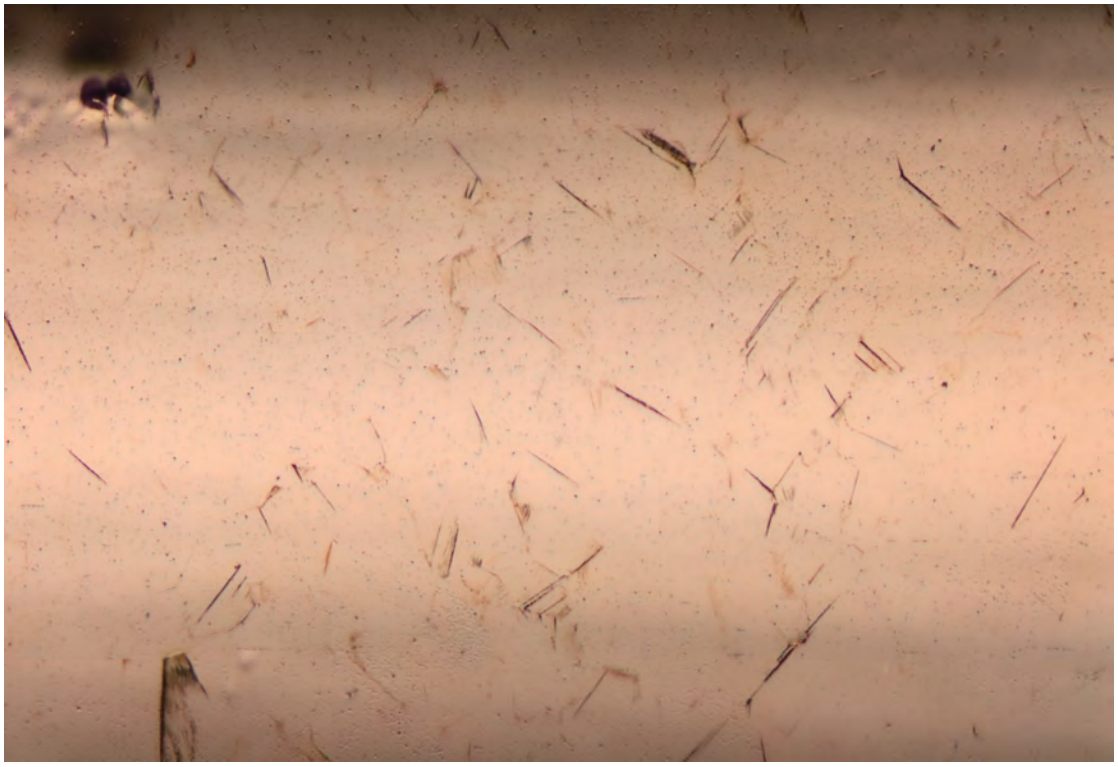

FIGURE E.12: Specimen N25 after training procedure $N = 0$ cycles.

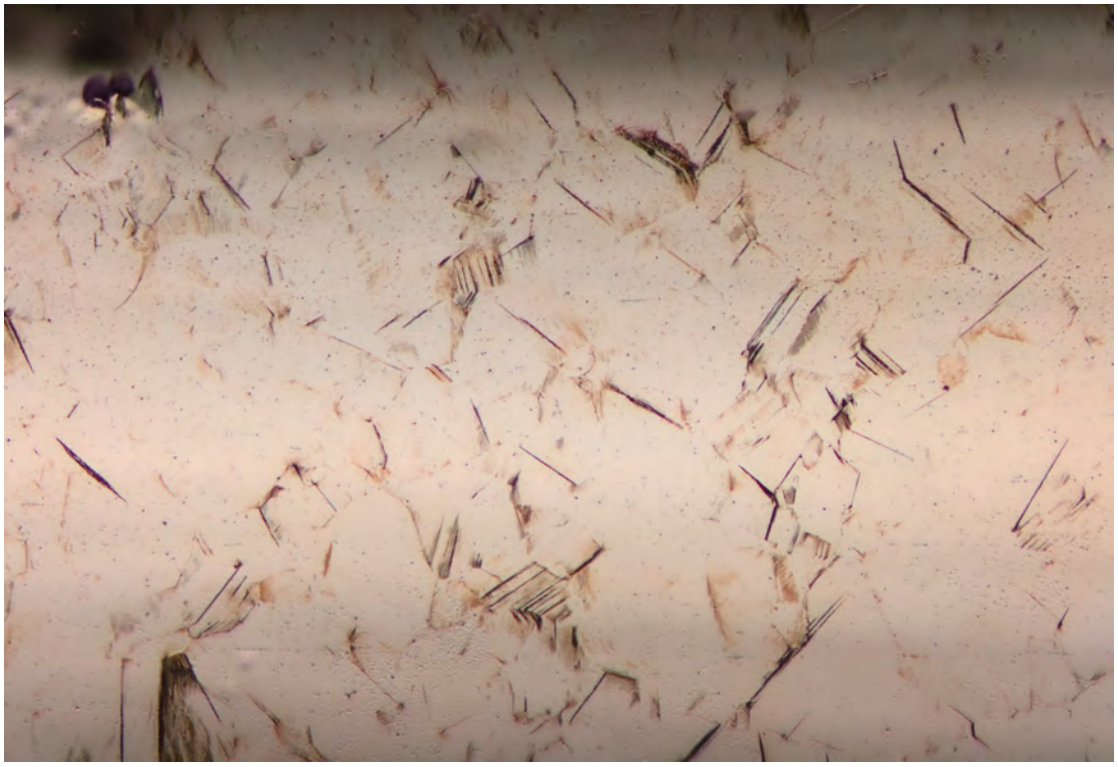

FIGURE E.13: Specimen U21 after $N = 8.10 \cdot 10^5$ cycles.

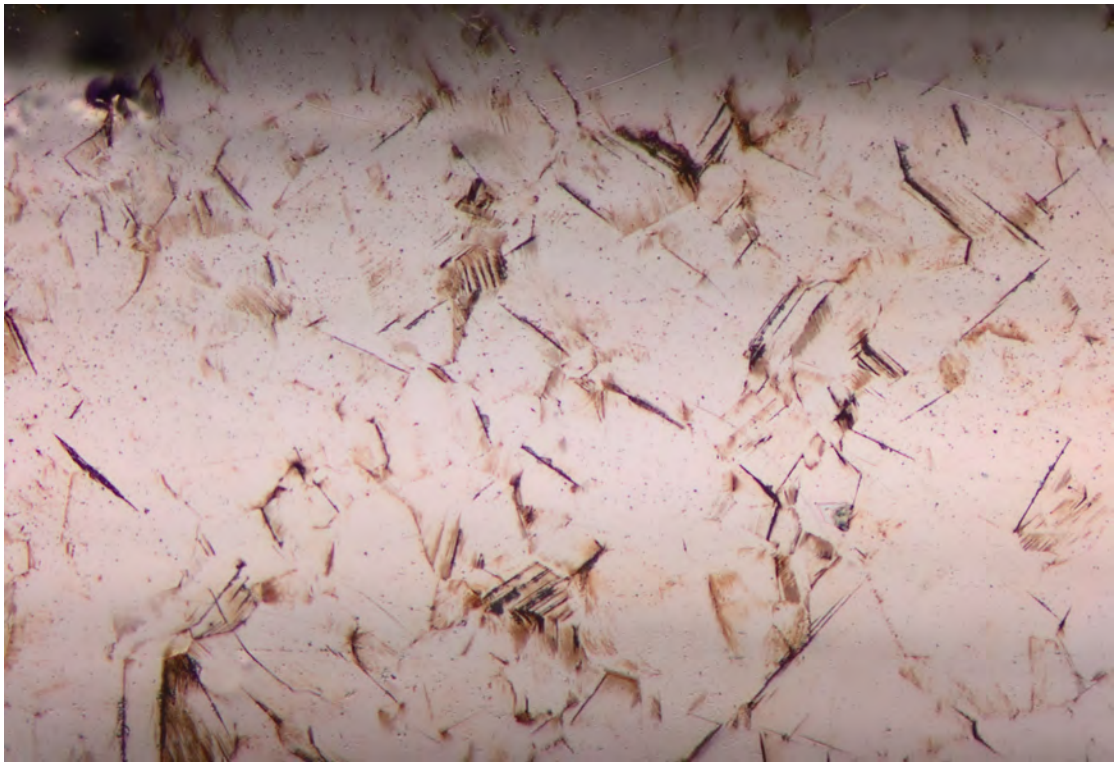

FIGURE E.14: Specimen U21 after $N = 1.62 \cdot 10^6$ cycles.

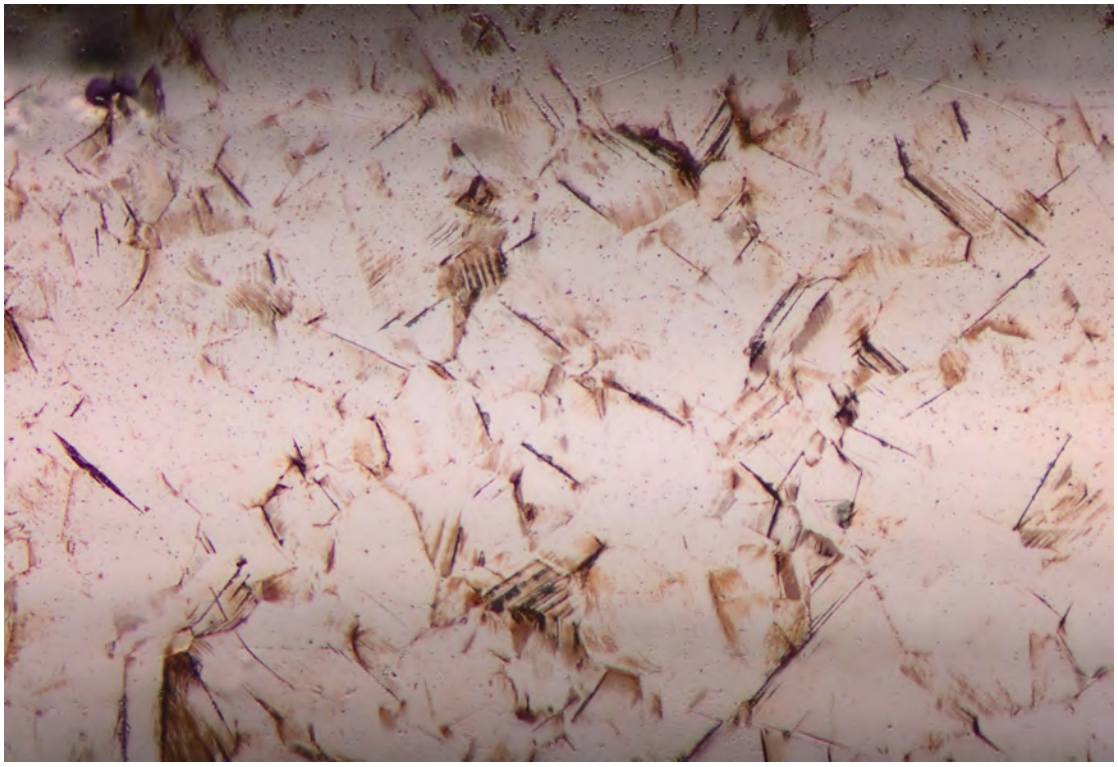

FIGURE E.15: Specimen N25 after $N = 2.43 \cdot 10^6$ cycles.

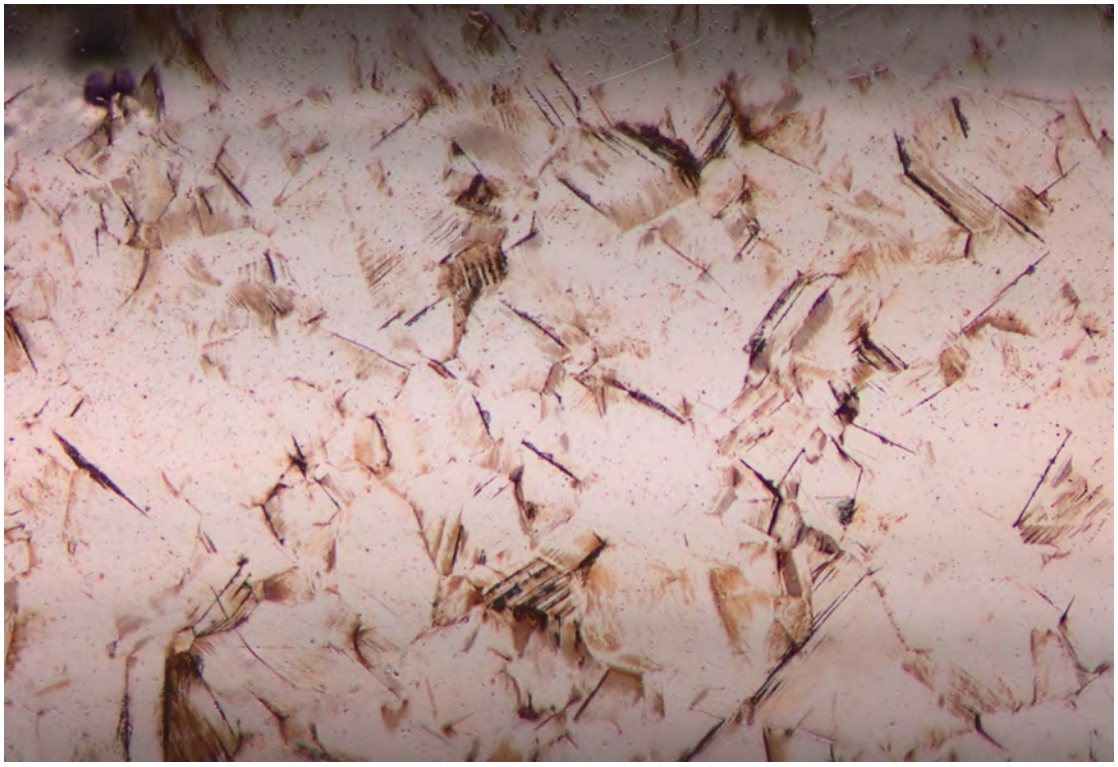

FIGURE E.16: Specimen U21 after $N = 3.24 \cdot 10^6$ cycles.

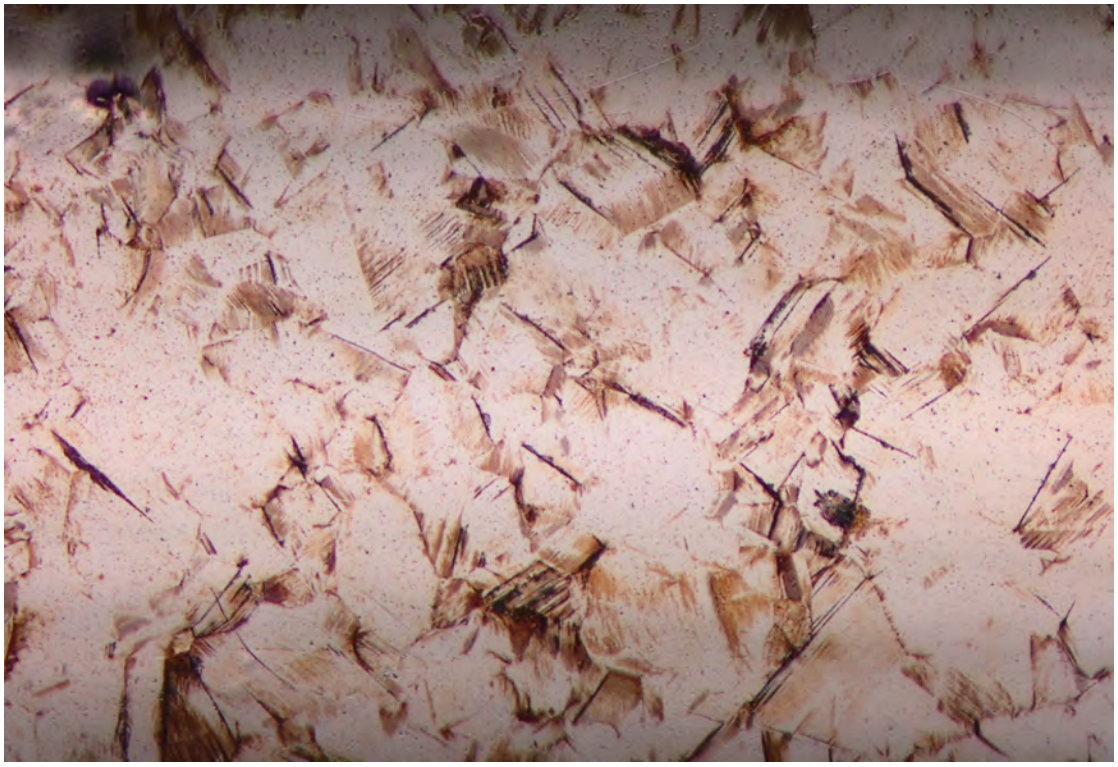

FIGURE E.17: Specimen U21 after $N = 4.05 \cdot 10^6$ cycles.

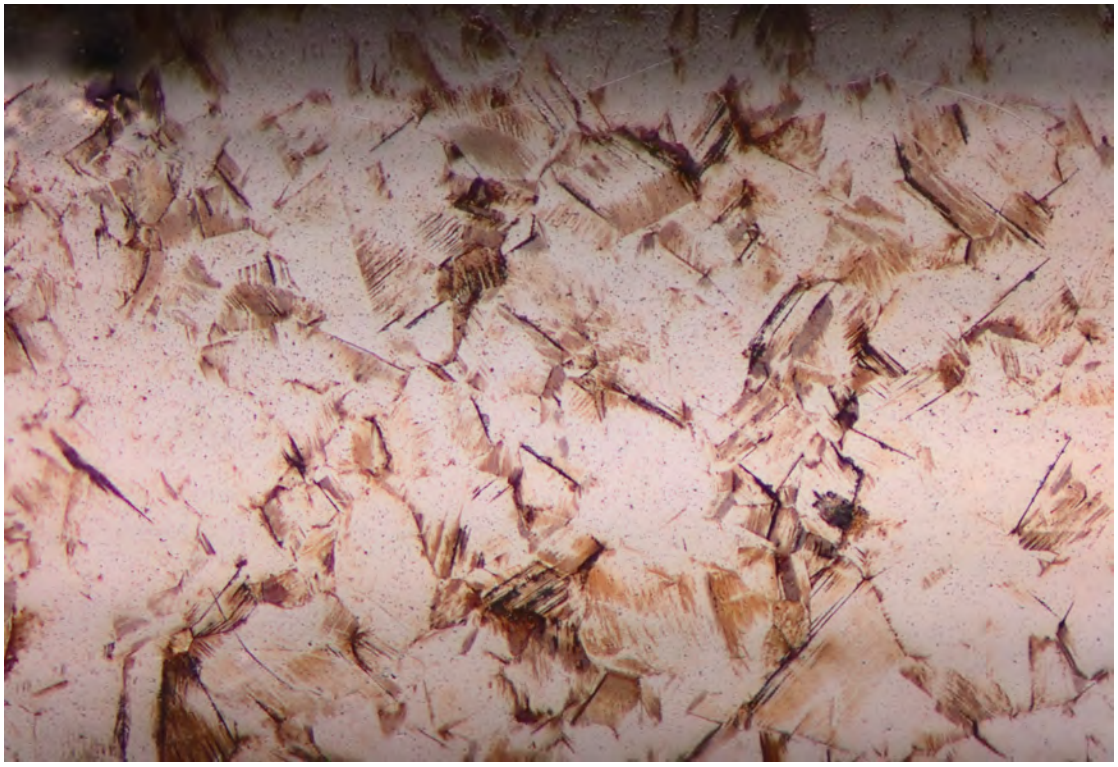

FIGURE E.18: Specimen U21 after $N = 4.86 \cdot 10^6$ cycles.

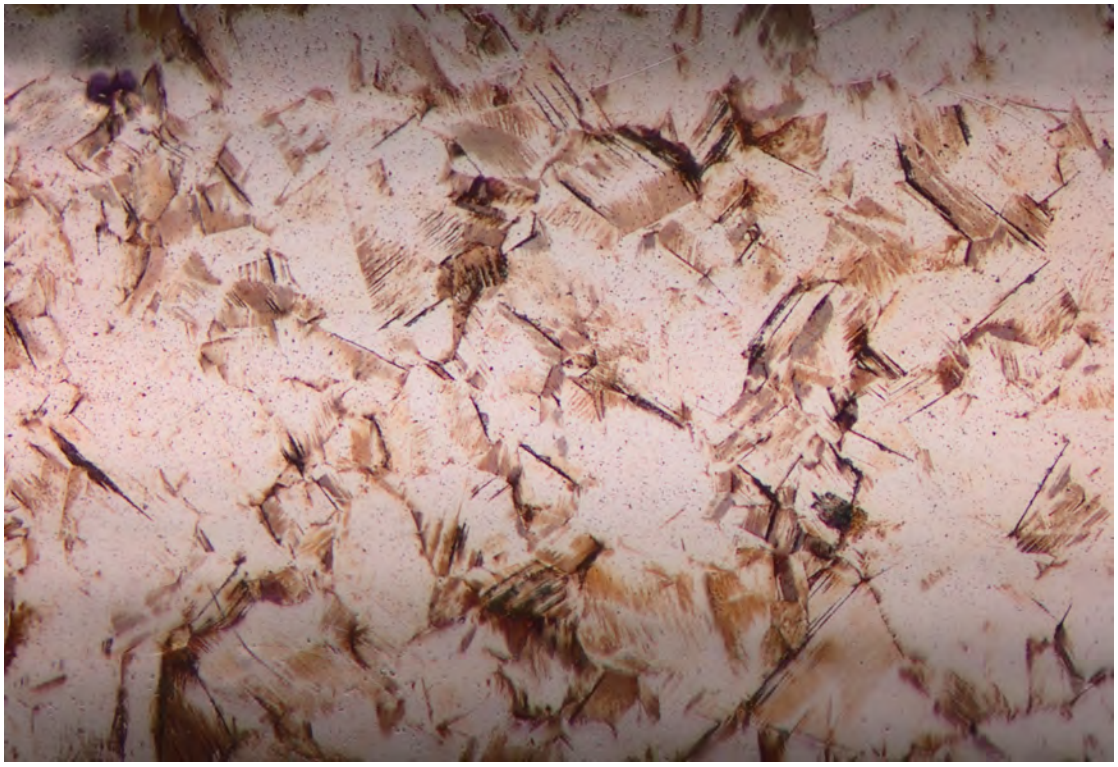

FIGURE E.19: Specimen U21 after $N = 5.67 \cdot 10^6$ cycles.

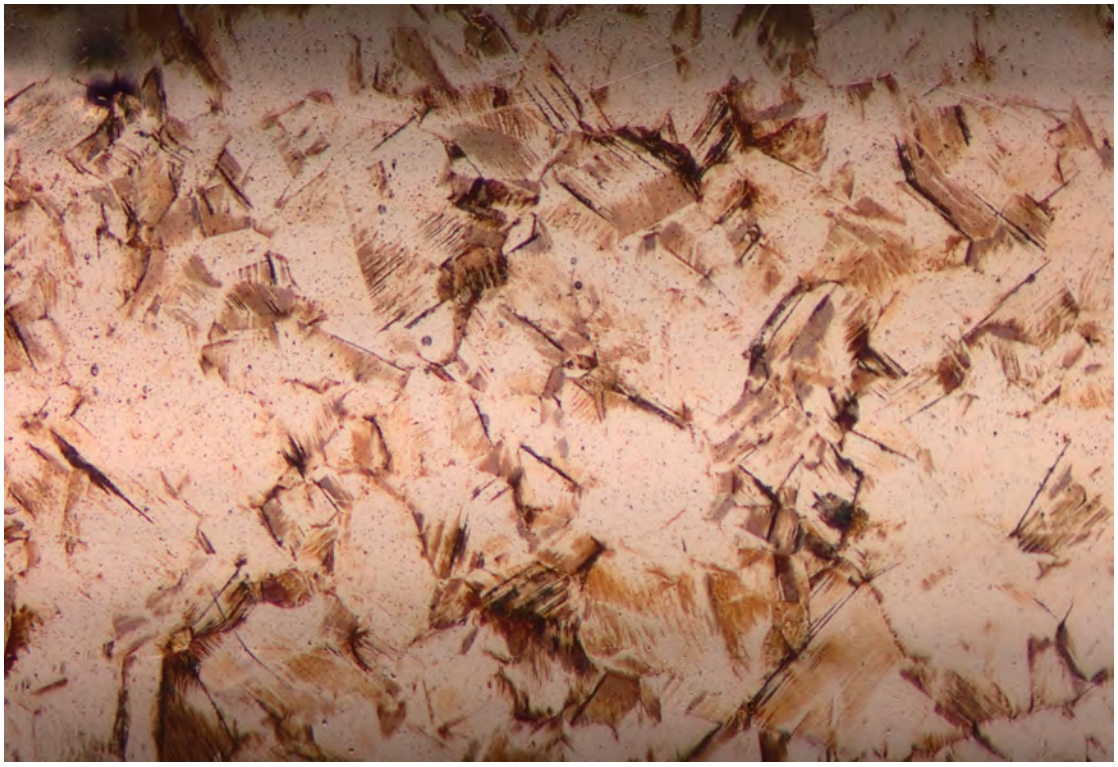

FIGURE E.20: Specimen U21 after $N = 6.48 \cdot 10^6$ cycles.

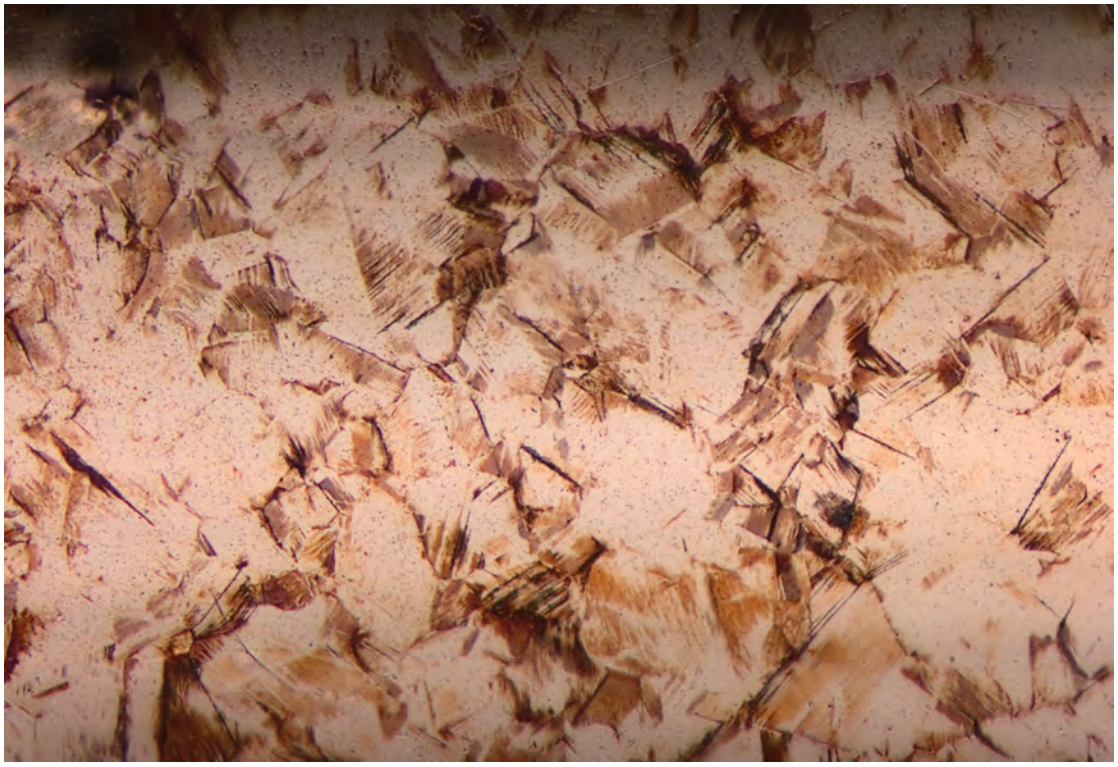

FIGURE E.21: Specimen U21 after $N = 7.29 \cdot 10^6$ cycles.

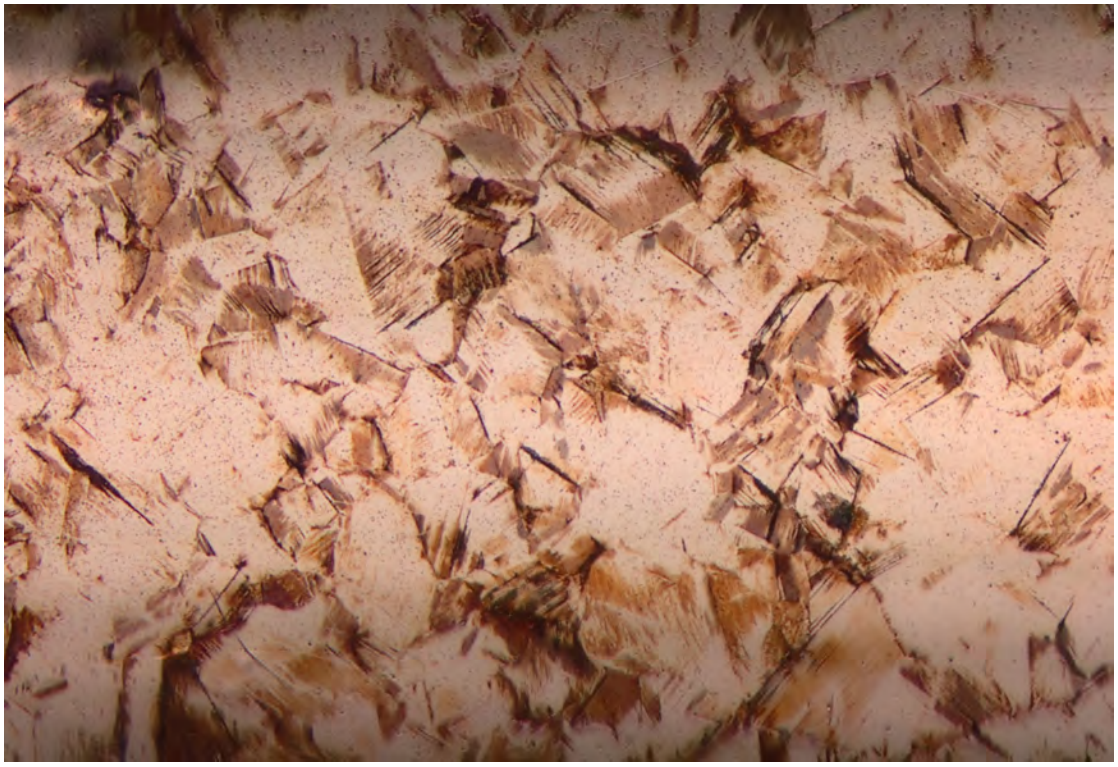

FIGURE E.22: Specimen U21 after $N = 8.10 \cdot 10^6$ cycles.

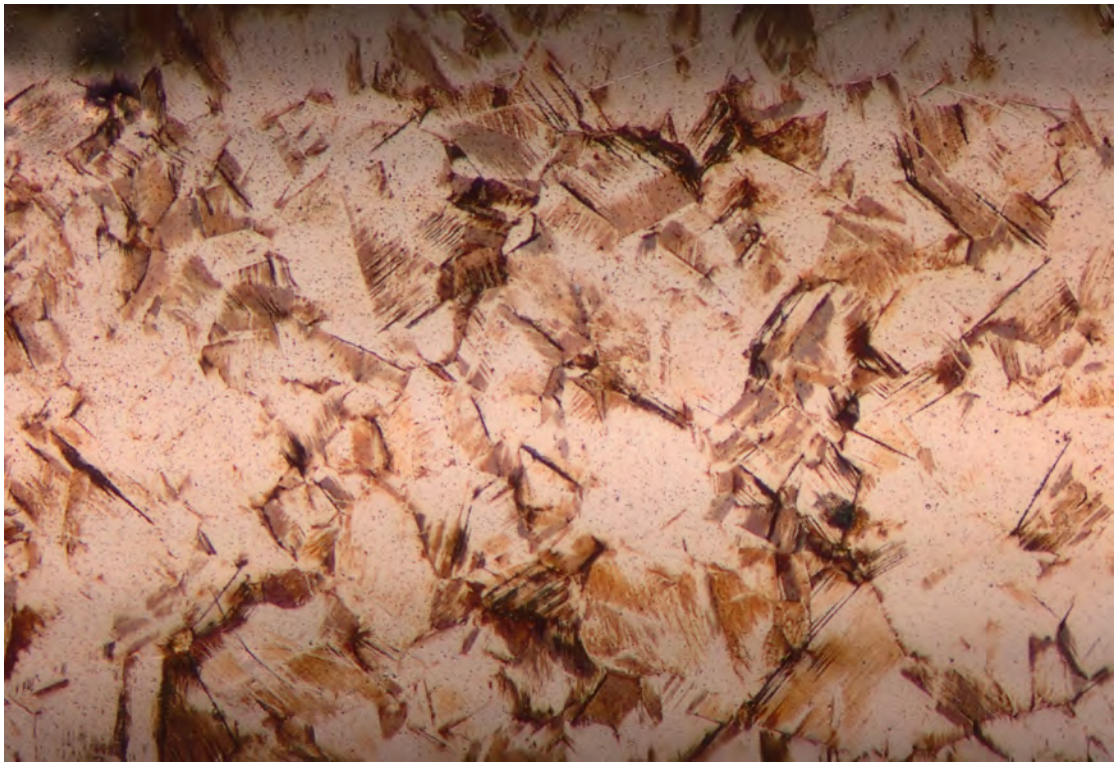

FIGURE E.23: Specimen U21 after $N = 8.91 \cdot 10^6$ cycles.